Nuclear magnetic resonance relaxation and diffusion in the presence of internal gradients: The effect of magnetic field strength

J. Mitchell,* T. C. Chandrasekera, M. L. Johns, and L. F. Gladden
Department of Chemical Engineering and Biotechnology, University of Cambridge, Pembroke Street, Cambridge CB2 3RA, United Kingdom

E. J. Fordham
Schlumberger Cambridge Research, High Cross, Madingley Road, Cambridge CB3 0HG, United Kingdom
(Received 19 November 2009; published 3 February 2010)

It is known that internal magnetic field gradients in porous materials, caused by susceptibility differences at the solid-fluid interfaces, alter the observed effective Nuclear Magnetic Resonance transverse relaxation times $T_{2,\mathrm{eff}}$. The internal gradients scale with the strength of the static background magnetic field B_0. Here, we acquire data at various magnitudes of B_0 to observe the influence of internal gradients on T_2-T_2 exchange measurements; the theory discussed and observations made are applicable to any T_2-T_2 analysis of heterogeneous materials. At high magnetic field strengths, it is possible to observe diffusive exchange between regions of local internal gradient extrema within individual pores. Therefore, the observed exchange pathways are not associated with pore-to-pore exchange. Understanding the significance of internal gradients in transverse relaxation measurements is critical to interpreting these results. We present the example of water in porous sandstone rock and offer a guideline to determine whether an observed $T_{2,\mathrm{eff}}$ relaxation time distribution reflects the pore size distribution for a given susceptibility contrast (magnetic field strength) and spin echo separation. More generally, we confirm that for porous materials T_1 provides a better indication of the pore size distribution than $T_{2,\mathrm{eff}}$ at high magnetic field strengths ($B_0 > 1$ T), and demonstrate the data analysis necessary to validate pore size interpretations of $T_{2,\mathrm{eff}}$ measurements.

DOI: 10.1103/PhysRevE.81.026101 PACS number(s): 89.90.+n, 02.60.Pn, 61.43.Gt, 07.55.−w

I. INTRODUCTION

Magnetic field gradients caused by susceptibility differences at material interfaces are a well-known phenomenon in Magnetic Resonance Imaging (MRI) and numerous imaging techniques exist to either eliminate or utilize this contrast mechanism [1]. The presence of these internal gradients in porous media is well known [2] although the influence on complex two-dimensional Nuclear Magnetic Resonance (NMR) relaxation time correlation measurements has not yet been explored. Early work on transition metal particles provided a demonstration of the link between susceptibility gradients and broadening of resonance lines in NMR experiments [3]. Since then, studies have been undertaken on the internal fields in randomly packed beds of glass spheres [4] and sedimentary rocks [5,6]. As with medical imaging, techniques have been proposed to circumvent the effects of susceptibility contrast in porous media, such as the quantitative Single Point Imaging (SPI) suite of measurements [7,8], or to exploit them, such as the Decay due to Diffusion in the Internal Field (DDIF) pulse sequence [9], which aims to determine pore size distributions from diffusion eigenmodes [10].

In this work, we are concerned with the influence of these internal gradients on two-dimensional NMR relaxation time measurements. Recently, correlations of relaxation time (T_1 and T_2) and self-diffusion coefficient (D_0) have become a popular method of probing pore structure, primarily in petrophysical applications [11–15]. Brownstein and Tarr first demonstrated that relaxation rates of confined liquids are proportional to the surface-to-volume ratio of pores [16]; these measurements were used subsequently to probe the microstructure of oil-bearing rocks [17] and determine pore size distributions by inverting the relaxation time data using nonnegative least-squares (NNLS) fitting algorithms [18] of varying complexity. This class of inversion techniques is referred to popularly in the literature as "Laplace inversions" although this is not a precise mathematical description of the method. Early work focused on longitudinal T_1 relaxation measurements (demonstrated elsewhere to be weakly dependent on magnetic field strength [19] and independent of internal gradients [20]) and so provided an accurate reflection of the pore structure. However, it is often more convenient, especially in oil-well logging applications [21], to use the transverse T_2 relaxation as a substitute for T_1 since the Carr-Purcell-Meiboom-Gill (CPMG) echo train pulse sequence [22,23] allows for the rapid acquisition of T_2 data. It is also common to acquire T_2 data in the second dimension of a two-dimensional data set since a CPMG echo train can be implemented after almost any NMR preconditioning of the system in the first dimension. However, spin echo measurements are known to be influenced by diffusion in magnetic field gradients [22,24] and so local variations in magnetic field strength B_0 can affect the acquired signal decay curves. At low magnetic fields ($B_0 < 50$ mT, typical for logging tools), the internal gradients can be negligible in sandstones [5], and the fixed magnetic field gradient inherent in unilateral well logging magnets determines the diffusive attenuation in the T_2 measurements [25,26]. In this paper, we discuss a method for estimating whether the distribution of $T_{2,\mathrm{eff}}$

*Corresponding author.jm600@cam.ac.uk

relaxation times reflects the pore size distribution when the observed transverse relaxation is dominated by molecular diffusion through the internal gradients. T_2-based measurements are now being used increasingly to study porous materials and these measurements are undertaken at various magnetic field strengths (dictated usually by the NMR system available). It is therefore timely to attempt to quantify the errors introduced when performing measurements at higher field strengths.

The two-dimensional T_2-T_2 relaxation exchange (REXSY) measurement [27–29] would be expected to be particularly susceptible to the effects of internal gradients as it relies on the analysis of echo train decays in both dimensions. First proposed by Lee *et al.* [30], the data analysis relies on a fast two-dimensional numerical inversion process that compresses the data into a linear Fredholm integral form [31]. The T_2-T_2 relaxation exchange measurement has been validated with water exchanging between layers of glass beads [32] and used to observe diffusive exchange in cement pastes [29] and sandstones [28]. It has also been combined with NMR propagator measurements [33] and used to explore pore connectivity in limestones [34] and biofilms [35]. These measurements have been made across a range of magnetic field strengths, although no consistent study has been attempted so far as to the influence of field strength—and hence internal gradients—on the correlation maps obtained from T_2-T_2 measurements. Here, we explore the interplay of internal gradients and diffusive exchange by obtaining relaxation exchange data from a water saturated sandstone core at various magnetic field strengths. Using this information, we suggest guidelines for implementing T_2 measurements of pore size distributions and T_2-T_2 exchange experiments, and estimate typical errors introduced if a suboptimal selection of parameters and field strength is employed.

The structure of the paper is as follows: in Sec. II, we review the literature on internal gradients and review extensive prior work on restricted diffusion under the conditions of bounded and unbounded magnetic fields. We expand on the concept of the so-called Localization regime [36] and hypothesize on the shape of magnetic field profiles in three-dimensional pores within this regime. The basic characterization of the physical rock structure is described in Sec. III. In Sec. IV, we describe the experimental NMR techniques employed. The experimental results are presented in Sec. V and are discussed in light of the theory in Sec. II.

II. THEORY

Here, we review the current theories for diffusion of fluids governed by molecular self-diffusion D_0 and restricted by solid boundaries, as found in porous media. These theories include NMR relaxation at surfaces observed via T_1 and T_2 processes. Additional loss of coherent magnetization occurs due to diffusion in magnetic field gradients, although this is only observed in measurements of T_2 relaxation. The common basis for T_2 relaxation is the Bloch-Torrey equation [37] describing the evolution of transverse magnetization $M(\mathbf{r},t)=M_x+iM_y$ in a magnetic field $B_z(\mathbf{r})$ that varies spatially as

$$\frac{\partial M}{\partial t} = D_0 \nabla^2 M(\mathbf{r},t) - i\gamma B_z(\mathbf{r}) M(\mathbf{r},t). \tag{1}$$

We observe the decay of the complex magnetization $M(\mathbf{r},t)$ in the heterodyne detection frame (corotating reference frame) at the resonance frequency $\omega_0=\gamma B_0$, where B_0 is the static magnetic field. This is equivalent to assuming $B_z(\mathbf{r})$ has a zero spatial average. Additionally, we ignore bulk relaxation. The initial (total) magnetization is $M_0=M(\mathbf{r},0)$. Where the field gradient $\mathbf{g}=\nabla B_z$ is uniform, and $B_z(\mathbf{r})=\mathbf{g}\cdot\mathbf{r}$. The term $D_0\nabla^2 M$ in Eq. (1) describes the dephasing of the spin ensemble as molecules diffuse from $\mathbf{r}$ to $\mathbf{r}'$ in the presence of a magnetic field gradient $g(\mathbf{x})$. A natural length scale arises: the dephasing length ℓ_g, defined as [25]

$$\ell_g = \left(\frac{D_0}{\gamma g}\right)^{1/3}. \tag{2}$$

This is the effective distance molecules must diffuse for their spins to dephase by 2π radians. For nonuniform gradients, ℓ_g defines a local quantity. A spatial average $\overline{g^2}$ defines a very similar length scale ℓ_G, such that

$$\ell_G = \left(\frac{D_0^2}{\gamma^2 \overline{g^2}}\right)^{1/6} = \left[\frac{D_0^2}{\gamma^2 \overline{(\nabla B_z)^2}}\right]^{1/6}. \tag{3}$$

The boundary condition at solid surfaces is

$$D_0 \frac{\partial M}{\partial \nu} + \rho M(\mathbf{r},t) = 0, \tag{4}$$

where $\partial/\partial\nu$ denotes the derivative normal to the surface and ρ is the surface relaxivity. This equation encompasses both restricted diffusion due to a surface (a "reflecting" boundary where $\rho=0$) and relaxation at surfaces determined by the value of ρ. The following discussions consider predominantly the special cases of (i) $\mathbf{g}=\mathbf{0}$ everywhere with $\rho\neq 0$ (surface relaxation only), and (ii) $\mathbf{g}\neq\mathbf{0}$ with $\rho=0$ (decay due to diffusion in a magnetic field gradient without surface relaxation).

A. Diffusion and surface relaxation in pores

The surface relaxation only case (simple diffusion without a magnetic field gradient) was analyzed by Brownstein and Tarr [16]. The observable magnetization $M(t)$ is a sum of exponential decay modes with positive relative intensities I_i

$$M(t) = M_0 \sum_{i=0}^{\infty} I_i \exp(-t/T_i), \tag{5}$$

where, in the context of NMR, the modal relaxation times T_i may be for either longitudinal (T_1) or transverse (T_2) relaxation processes. For pores of particular volume-to-surface ratio $V/S=a$, two asymptotic regimes were identified [16].

(a) The "fast-diffusion" or "weak relaxation" regime where $\rho a/D_0 \ll 1$. The relaxation is unimodal; only I_0 is significant. Any given pore size contributes only one relaxation time to the magnetization decay. The fluid is well-mixed and the magnetization remains uniform across the pore during the decay.

(b) The "slow diffusion" or "strong relaxation" regime where $\rho a/D_0 \geqslant 10$. Relaxation is multimodal; I_0 is the largest intensity (61% for spherical pores [16]) but the higher modes ($i>0$) are non-negligible. Each pore size contributes several relaxation times to the overall signal. There is poor mixing between the surface and bulk; magnetization across the pore is nonuniform.

Between these limits, where $1 \ll \rho a/D_0 \ll 10$, the lowest mode I_0 is dominant, but the single-mode behavior fails.

In polydisperse porous media (including sedimentary rocks), observed multiexponential relaxation can be interpreted as a distribution of pore sizes when the "fast-diffusion" behavior dominates [17]. This interpretation associates relaxation times with pore sizes using surface relaxivity as a scaling factor such that $a=\rho_{(1,2)}T_{(1,2)}$. Multimode behavior, i.e., the "slow diffusion" limit, would prevent such a simple interpretation, as observed in ideal systems [38]. In addition to the fast-diffusion limit (the normal case for sedimentary rocks) the conversion of relaxation time to pore size also requires that the pores act independently, an assumption that cannot be rigorous. Notwithstanding, this "fast-diffusion, independent pores" model remains the reference case for interpretation of NMR relaxation data in petrophysics [39] and analysis of other porous media.

B. Diffusion in uniform magnetic field gradients

The analysis of signal decay due to molecular diffusion through a nonuniform magnetic field is a complicated problem that has received much attention, motivated by several applications. In any real system, there will be some magnetic field inhomogeneity: in stray-field, "mobile," or "inside-out" NMR applications [40], including oil-well logging tools [21], strong magnetic field gradients may be inherent. Pulsed field gradients are used in imaging or diffusion measurements [41]. Here, we are concerned primarily with "internal gradients" induced by the mismatch in magnetic susceptibility $\Delta\chi$ between the solids and fluids.

First, we review the available results for uniform magnetic field gradients g (unbounded fields), then for simple models of bounded internal (induced) fields, and finally, heuristic approaches to real porous media with the inclusion of surface relaxation. The majority of the published theory covers the case of $\rho=0$.

The base case of unrestricted diffusion in a uniform gradient g was analyzed in the pioneering work of Hahn [24] where, for a single (Hahn) spin echo occurring at time 2τ, the diffusion leads to a magnetization decay exponent that varies with τ^3. The observation of unrestricted diffusion in T_2 measurements has been discussed in numerous works [22,37,42,43]. For fluids confined in pores (i.e., subject to restriction), this remains the asymptotic short-time (ST) limit, for echo times that are sufficiently short. The range of the ST regime is determined by the relative sizes of three significant length scales: the diffusion length $\ell_E=(D_0\tau)^{1/2}$, a structural length scale ℓ_s (equivalent to pore size for a defined pore geometry), and the dephasing length ℓ_g as defined above.

Three notable asymptotic regimes are identified in the literature [25,44,45], governed by whichever of the three length scales is shortest. The ST regime (which can be treated as unrestricted diffusion) applies when $\ell_E \ll \ell_s, \ell_g$ [45]. This behavior breaks down whenever ℓ_E exceeds either ℓ_s or ℓ_g. The long-time asymptotic behavior has two limiting cases, depending on the relative size of ℓ_s and ℓ_g [44]. These cases may be referred to as "fast" and "slow" diffusion [36] in analogy with the analysis of surface relaxation discussed above [16].

The fast-diffusion case occurs when $\ell_s \ll \ell_g, \ell_E$ (typical for small pores) [36,43,46]. In this regime, spins explore the entire pore many times before dephasing has occurred, so any local magnetic field variations are averaged out by diffusion. For this reason, the more usual name for this case is the Motional Averaging (MAV) regime [25]. Unlike the ST regime, where magnetization decays faster for higher D_0, magnetization decays slower for higher D_0 in the MAV regime because the averaging is more effective. As in the fast-diffusion regime for surface relaxation, magnetization is uniform over the pore in both the ST and MAV limits. Another common feature of the MAV regime is that the spin phase distribution is Gaussian [47]; the so-called Gaussian Phase Approximation (GPA) is used frequently in analyses of both these regimes [48].

The slow diffusion case occurs when $\ell_g \ll \ell_s, \ell_E$ [36]. This is typical for strong magnetic field gradients in large pores. Due to the cube root dependence on g in Eq. (2), typical values for ℓ_g in experiments tend to range over the rather small span $\sim 1-10$ μm [25]; this is relevant for many rocks. In this slow diffusion case, spins dephase by more than 2π radians before they encounter pore walls. Significant coherent magnetization will only survive in molecules in close proximity to pore walls due to the restriction on diffusive motion. In this regime the GPA fails and magnetization is nonuniform across the pore. This inspires the usual name of the localization regime to describe this asymptotic behavior.

These regimes were analyzed first for the case of the single (Hahn) echo in a uniform magnetic field gradient [25,44,45,48]. However, regimes of similar qualitative characteristics appear in analysis of more general situations: multiple echoes in a CPMG train, and nonuniform gradients both bounded and unbounded. We consider in turn these cases of increasing complexity, starting with available results for uniform g.

In the ST regime, the generalized magnetization decay with first order corrections due to restriction is [47,49]

$$\frac{M(2n\tau)}{M_0} = \exp\left\{-\frac{2}{3}\left(\frac{\ell_E}{\ell_g}\right)^6\left[n - C(n)\frac{\ell_E}{\ell_s}\right]\right\}, \tag{6}$$

where $C(n)$ represents restriction dependent coefficients of echo order n. The leading term of the decay exponent can be expressed in length scale ratios or dimensional parameters as

$$\frac{2}{3}n\left(\frac{\ell_E}{\ell_g}\right)^6 = \frac{2}{3}\gamma^2\overline{g^2}D_0 n\tau^3 = \frac{1}{12}\gamma^2\overline{g^2}D_0 t_E^2 t. \tag{7}$$

Equation (6) encompasses both the classic Hahn echo ($n=1$) and CPMG echo train ($n>1$) experiments for unrestricted diffusion. The relevant diffusion length is $\ell_E=(D_0\tau)^{1/2}=(D_0 t_E/2)^{1/2}$ and we use this notation to emphasize

that it is diffusion during one echo interval, not total elapsed (CPMG) time, that determines the relevant length scale. The leading term remains valid even for nonuniform fields, although the restriction correction is modified by certain moments of the magnetic field variation [49]. The coefficients $C(n)$ have been tabulated up to $n=40$ for restriction in one dimension [47]. For $n=1$, the restriction correction has been given [36] for an arbitrary pore shape and three-dimensional restriction in the form $C(1)(\ell_E/\ell_s)=\alpha(S/V)\ell_E$ where $\alpha \simeq 0.314$.

In all these cases, the key feature of the ST regime (accessible by experimentation) is the dependence of the decay exponent on τ^3, or in multiecho trains on echo time $t_E^2 t$, not just elapsed time t. Dependence of decay on t_E is the most common experimental test for significant field gradients [5].

In the MAV regime, a general result for one-dimensional restrictions has been given [47] where the leading term of the decay exponent is

$$\frac{2n}{120}\left(\frac{\ell_E^2\ell_s^4}{\ell_g^6}\right)=\frac{1}{60}\frac{\gamma^2 g^2 \ell_s^4}{D_0}n\tau=\frac{1}{120}\frac{\gamma^2 g^2 \ell_s^4}{D_0}t. \tag{8}$$

The critical features are a strong dependence on pore size ℓ_s, inverse dependence on D_0, and linearity with τ. There is no dependence on echo time t_E for multiecho measurements. Note that this means an absence of t_E dependence cannot be taken as strong evidence for the absence of internal gradients, as noted already in [50]. For $n=1$, the results for slab, cylindrical, and spherical geometries were given by Neumann [48]. For a sphere of radius R_p, the result for $n=1$ is retrieved by the substitutions $\ell_s \to R_p$ and $1/120 \to 8/175$ in Eq. (8). The dependence on the fourth power of the structural length is similar. However, a weaker power law applies for bounded fields as discussed below.

Finally, in the localization regime, the most general result for CPMG and one-dimensional restriction is [47]

$$\frac{M(2n\tau)}{M_0} \sim p(n)\frac{\ell_g}{\ell_s}\exp\left[-a_1 n\left(\frac{\ell_E}{\ell_g}\right)^2\right], \tag{9}$$

where $p(1)\simeq 5.88$; a generating formula for $p(n)$ has been given elsewhere [47]. The coefficient $a_1 \simeq 1.02$ is the first zero of the Airy function derivative $\mathrm{Ai}'(x)$. In this regime, the pre-exponential factors are important. The ratio ℓ_g/ℓ_s represents, approximately, the fraction of pore volume containing coherent magnetization. The analysis for $n=1$, including two and three-dimensional restriction, has been discussed by de Swiet and Sen [36]. The decay exponent can be expressed in dimensional parameters as

$$-a_1 n\left(\frac{\ell_E}{\ell_g}\right)^2 = -1.02\gamma^{2/3} g^{2/3} D_0^{1/3}\frac{t}{2}, \tag{10}$$

and is universal for one-dimensional restriction, independent of pore size, and depends only weakly on D_0. For three-dimensional restriction, a similar asymptotic behavior is predicted [36], independent of both pore size and details of pore shape.

The localization regime was verified experimentally for one-dimensional restriction and $n=1$ [25], with similar behavior observed in earlier data [43]. We know of no such demonstration for restriction in two or three dimensions. For restriction in the higher dimensions, it is argued that the asymptotic behavior may not be observable except at vanishingly small signal levels [36]. This is because the dominant behavior of the magnetization is governed by the pre-exponential factor. The preasymptotic localization regime remains important: however, the GPA will still fail and magnetization becomes nonuniform for times outside of the ST approximation, and well before the universal decay is expected to be observed. An intermediate range of times $(\gamma g)^{2/3} D_0^{1/3} < \tau < (R_p/\gamma g D_0)^{1/2}$ is predicted [36] (for $n=1$) for which the decay exponent has neither pure τ^3 nor pure τ dependence. We conjecture, therefore, that some remaining dependence on t_E exists for the CPMG experiment ($n>1$), for restriction in two or three dimensions governed by the preasymptotic localization regime.

C. Diffusion in bounded and internal magnetic field gradients

Most of the conditions discussed above are for the case of uniform g. Some general results are known for nonuniform magnetic fields (e.g., the ST regime [49]) where an important distinction exists between bounded and unbounded fields. Unbounded fields are exemplified by gradients imposed by the apparatus. In this paper, the induced internal magnetic field variations are of primary importance. Induced internal gradients may become very large, but the overall field variations are bounded by $\pm\Delta\chi B_0/2$, approximately [51].

Some theoretical equations are available for a cosine profile in a one-dimensional restriction that may taken as a crude model for the internal magnetic field variation in a porous medium [49]. Here, the field variation over ℓ_s is

$$B_z(x) = \Delta\chi B_0 \cos\left(\frac{\pi x}{\ell_s}\right), \tag{11}$$

and the spatial average dephasing length ℓ_G is

$$\ell_G^3 = \frac{\sqrt{2}}{\pi}\frac{D_0\ell_s}{\Delta\omega_0}, \tag{12}$$

where $\Delta\omega_0=\gamma\Delta\chi B_0$. This model has local field variations, bounded by $\pm\Delta\chi B_0/2$, corresponding to a spread in Larmor frequencies $\Delta\nu_0=\gamma\Delta\chi B_0/\pi$ where $\Delta\nu_0$ may be taken as a line width, ignoring numerical factors of order 1. The implied line shape is bimodal and not representative of the Lorentzian line shape observed empirically for most natural porous media [52].

In the ST regime, the general result is similar to Eq. (6) with modifications to the leading restriction correction in terms of two moments of the field variation. For the cosine model, the restriction correction of order ℓ_E/ℓ_s becomes of order $(\ell_E/\ell_s)^2$ [49]. For field variations with an odd reflection symmetry, such as $\sin(\pi x/\ell_s)$, the restriction correction is the same as for the case of uniform g [49].

In the MAV regime, the leading term of the decay exponent for the cosine model is

$$\frac{2n}{\pi^4}\left(\frac{\ell_E^2\ell_s^4}{\ell_g^6}\right)=\frac{1}{\pi^2}\frac{(\Delta\omega_0)^2\ell_s^2}{D_0}t, \tag{13}$$

where the dependence on ℓ_s^2 is not as strong as the ℓ_s^4 dependence for the uniform magnetic field case. A higher order correction is given elsewhere [49]. A heuristic approach (see references [25,49,53] and discussion below) shows this ℓ_s^2 dependence occurs for more general bounded magnetic fields.

Finally, in the localization regime, the asymptotic behavior is shown to be sensitive to particular details of the magnetic field inhomogeneities. This is not the case for either the ST or MAV regimes [49]. In the cosine field for one-dimensional restriction only, the asymptotic localization behavior is [49]

$$\frac{M(2n\tau)}{M_0}\propto\exp\left[-(2\pi^2)^{1/4}n\left(\frac{\ell_G}{\ell_s}\right)^{1/2}\left(\frac{\ell_E}{\ell_G}\right)^2\right], \tag{14}$$

with pre-exponential factors reflecting the volume fraction of surviving magnetization, as in Eq. (9). The exponent can be expressed in dimensional parameters as

$$-(2\pi^2)^{1/4}n\left(\frac{\ell_G}{\ell_s}\right)^{1/2}\left(\frac{\ell_E}{\ell_G}\right)^2=-\pi\frac{(\Delta\omega_0)^{1/2}}{\ell_s}D_0^{1/2}\frac{t}{2}. \tag{15}$$

Although linear with τ, this regime is no longer universal, being dependent on the structural length scale (pore size) ℓ_s. It has been conjectured that this ℓ_s dependence is a general feature of bounded fields [49]. We do not know of any asymptotic analysis in two or three-dimensional geometry for the cosine or other bounded field models, nor for one-dimensional restriction with bounded field models of the opposite symmetry (e.g., a sine-like magnetic field). However, the solutions to such models would be informative (i) because of the possibility of local regions of weak gradients around magnetic field extrema within the pores and away from the pore walls, and (ii) because of the need to examine the ranges of τ for which asymptotic behavior is expected, as in Eq. (14). By analogy with the arguments in [36], it is reasonable to expect a range of τ times for which the magnetization decay is neither τ^3 (ST regime) nor τ (asymptotic localization regime) dependent. Such conjecture is strengthened by the possibility of regions of surviving magnetization around field extrema within the pore, which may be expected reasonably to exhibit unrestricted diffusion behavior (i.e., τ^3 or $t_E^2 t$ dependence) for a wider range of τ times than for regions of magnetization found close to the pore walls.

Even for regular porous media models, induced magnetic field profiles are not simple [54]. For natural, irregular porous media, field variations will not be expressible by any simple model, and a heuristic approach is necessary [5]. However, the bounded field character remains and some general principles may be identified. The concepts of the ST, MAV, and localization regimes of magnetization decay in bounded fields are still applicable [5].

The ST behavior is expected to be observed in large pores, although the length scale for which the term "large" applies needs to be quantified. Elsewhere, the concept of an effective gradient g_{eff} was introduced [5] such that for a volume of spins with characteristic size ℓ_c [36], the variation in Larmor frequency $\delta\omega_0(x)\simeq\gamma g_{\text{eff}}\ell_c$, and this should be equal to the uncertainty caused by diffusion across a length on the order of D_0/ℓ_c^2 (i.e., the reciprocal diffusion time required for a molecule to cross ℓ_c). Hence,

$$\ell_c(x)=\left(\frac{D_0}{\gamma g_{\text{eff}}(x)}\right)^{1/3}, \tag{16}$$

which is simply a local version of the dephasing length ℓ_g, using an effective gradient instead of point values of $g(x)$. On length scales finer than ℓ_c, the details of $g(x)$ become unimportant because of the averaging imposed by diffusion. For a given magnetic field gradient profile $g(x)$, the effective gradient is found in principle by averaging over ℓ_c, consistent with Eq. (16), such that $\ell_c g_{\text{eff}}=\int_0^{\ell_c}g(x)\mathrm{d}x$. This can be achieved only for explicit field models and not for arbitrary, unknown variations. However, even in the case of arbitrary magnetic field variations, some important general features can be deduced [5]. The internal fields are bounded such that $\ell_c g_{\text{eff}}\leq\Delta\chi B_0$ [51]. This equality determines a maximum value $g_{\max}$ for the effective gradient g_{eff} and a corresponding length scale ℓ_* so,

$$\ell_* g_{\max}=\Delta\chi B_0, \tag{17}$$

where ℓ_* and $g_{\max}$ are also constrained by $\ell_*=(D_0/\gamma g_{\max})^{1/3}$, yielding [5]

$$\gamma g_{\max}=\frac{(\gamma\Delta\chi B_0)^{3/2}}{D_0^{1/2}}, \tag{18}$$

$$\ell_*=\left(\frac{D_0}{\gamma\Delta\chi B_0}\right)^{1/2}. \tag{19}$$

The scaling of $g_{\max}\propto B_0^{3/2}$ is stronger than $g_{\max}\propto B_0$ expected, naïvely, from magnetostatics. It should be noted that $g_{\max}$ is (i) still an effective gradient where diffusive averaging of fine features is considered and not a point value $g(x)$, and (ii) a maximum value. This $B_0^{3/2}$ scaling is of importance in the selection of optimal field strengths for NMR analyses of porous media.

The length scale ℓ_* sets a limit on pore size for observing ST behavior. This is expected only for $\ell_s\geq\ell_*>\ell_E$. As such, ℓ_* differentiates between "small" and "large" pores. For $\ell_s<\ell_*,\ell_E$, motional averaging is expected to be observed. If $\ell_s<\ell_*$ but also $\ell_E<\ell_s$ then the ST behavior would be expected to be observed even in "small" pores. In practice, this may be outside achievable experimental parameters. Similarly, if $\ell_s\geq\ell_*$, but $\ell_E>\ell_*$, then ℓ_* becomes the shortest length. Analogous to all previous analyses, we would expect to observe the localization behavior, including failure of the GPA, nonuniform magnetization, sensitivity to details of the internal fields, and other features of this regime considered in the various models. We argue below that at high magnetic fields, the value of ℓ_* may become less than the minimum ℓ_E available experimentally. In such situations, the conditions for ST behavior cannot be satisfied, and we must expect the typical features of the localization regime to be apparent.

The use of ℓ_* as a discriminator for the ST and localization regimes is convenient in natural porous media because it

is independent of pore size. Where models such as the cosine magnetic field profile are applicable, the usual discriminator would be ℓ_G as defined in Eq. (12). We note that in the cosine field case $\ell_G^3=(\sqrt{2}/\pi)\ell_*^2\ell_s$, then this depends on ℓ_s. This is not a contradiction since for $\ell_s>\ell_*$, $\ell_s^3>\ell_*^2\ell_s\sim\ell_G^3$, and hence $\ell_s>\ell_G$. The same argument applies when $\ell_s<\ell_*$, leading to $\ell_s<\ell_G$. Assignments of diffusion regimes made using ℓ_G should be similar to those using ℓ_*.

The bounded field arguments can also be applied [49,53] to the MAV regime. The leading term in the decay exponent for the MAV regime (regardless of whether g is uniform or not) is of the form

$$-2n\frac{\ell_E^2\ell_s^4}{\ell_G^6}=-(\gamma^2\overline{g^2}\ell_s^2)\left(\frac{\ell_s^2}{D_0}\right)2n\tau, \tag{20}$$

omitting a geometry-dependent numerical factor of about 1/100. The factor $\gamma^2\overline{g^2}\ell_s^2$ is, according to the bounded field arguments, the total spread in frequency and can be approximated by $(\gamma\Delta\chi B_0)^2$, while ℓ_s^2/D_0 is the characteristic diffusion time required for a molecule to cross the pore. Hence, the decay exponent is proportional to

$$-(\gamma\Delta\chi B_0)^2\frac{\ell_s^2}{D_0}2n\tau=-\frac{\ell_s^2}{\ell_*^4}D_0t, \tag{21}$$

which confirms on a more general basis the ℓ_s^2 dependence found in the specific model of the cosine magnetic field profile. It is also clear that magnetization decay governed by the MAV regime is not dependent on t_E. Hence, this signal decay cannot be distinguished (in a CPMG measurement) from surface relaxation occurring simultaneously, although the dependence on ℓ_s is quite different (surface relaxation exponents scale inversely with ℓ_s). This indicates that diffusive decay is most important (relative to surface relaxation) in the largest pores governed by motional averaging.

We know of no general bounded field analyses for the localization regime. It has been shown [49] that the decay exponent for the localization behavior is sensitive to the details of the magnetic field profile. We conjecture, therefore, by analogy with the bounded field argument for the MAV regime, that in Eq. (20), we may replace $\gamma^2\overline{g^2}\ell_s^2$ by $(\gamma\Delta\chi B_0)^2$ as previously, obtaining for the decay exponent $-(\gamma\Delta\chi B_0)^{1/2}D_0^{1/2}t/\ell_s$ with some numerical factor expected to depend on pore shape. Curiously, the dependence on pore size here is identical to that expected for surface relaxation, but with a scale factor controlled by susceptibility contrast $\Delta\chi$, rather than surface relaxivity ρ. We emphasize that it remains unclear whether this asymptotic localization regime (with a decay exponent that varies linearly with τ) will ever be observed experimentally for general restrictions in two or three dimensions [36].

D. Diffusion in magnetic field gradients with surface relaxation

We now reintroduce surface relaxation. To interpret relaxation time in terms of pore sizes, we require surface relaxation to be the dominant process. From the discussions given above, it is clear that this condition will not always be satisfied experimentally. Observed transverse relaxation rates $1/T_{2,\mathrm{eff}}$ will be sums of surface and diffusive relaxation rates. In the ST regime, we expect (to leading order) [55]

$$\frac{1}{T_{2,\mathrm{eff},i}}\simeq\frac{1}{T_{2,i}}+\frac{D_0\gamma^2g_{\mathrm{eff},i}^2t_E^2}{12}=\frac{\rho_2}{a}+\frac{D_0\gamma^2g_{\mathrm{eff},i}^2t_E^2}{12}, \tag{22}$$

where i indexes pores of a particular size and $a=V/S$ is independent of pore shape.

In the MAV regime, we may write

$$\frac{1}{T_{2,\mathrm{eff},i}}\simeq\frac{1}{T_{2,i}}+\frac{(\gamma\Delta\chi B_0)^2R_p^2}{120D_0}=\frac{2\rho_2}{\ell_s}+\frac{(\gamma\Delta\chi B_0)^2\ell_s^2}{120D_0}, \tag{23}$$

where we use the bounded field arguments from above and approximate further numerical factors by unity. For consistency, the one-dimensional pore model is made explicit in the surface term to show the differing dependencies on ℓ_s. However, without other data, such models are unhelpful since we have no means of distinguishing surface relaxation from diffusive decay. We note that diffusive decay may be dominant in the largest small pores, while surface processes will dominate eventually in the smallest pores.

In the asymptotic limit of the localization regime, we might expect

$$\frac{1}{T_{2,\mathrm{eff},i}}\simeq\frac{1}{T_{2,i}}+\frac{(\gamma\Delta\chi B_0)^{1/2}D_0^{1/2}}{\ell_s}, \tag{24}$$

using the bounded field conjecture given above, again ignoring numerical factors of $\mathcal{O}(1)$. As for the MAV regime, there is no t_E dependence in this model; surface relaxation and diffusive processes would not be distinguishable in the relaxation data. We reiterate that this model is conjectural since it is unclear that the asymptotic localization regime will be explored experimentally for general pore geometries. Furthermore, magnetization in the localization regime is nonuniform, corresponding to the "slow diffusion" limit of Brownstein and Tarr [16]. It is therefore inconsistent to apply models for surface relaxation dependent on uniform magnetization, although surface processes are unlikely to be dominant even in this case. Somewhat more likely is a preasymptotic localization regime in which some dependence on t_E remains, while surface relaxation becomes unimportant. In the current literature, no models exist to describe this situation.

A distribution of large pores will have its own distribution of g_{eff}, say $f(g_{\mathrm{eff}})$. This will not necessarily be the same as the distribution $h(T_2)$ of surface relaxation times. In fact, it has been assumed previously that they are uncorrelated [5], leading to

$$\frac{M(t,t_E)}{M_0}\simeq\int\mathrm{d}T_2h(T_2)\int_0^{g_{\max}}\mathrm{d}g_{\mathrm{eff}}f(g_{\mathrm{eff}})\times\exp\left(-\frac{1}{12}D_0\gamma^2g_{\mathrm{eff}}^2t_E^2t\right)\exp\left(-\frac{t}{T_2}\right), \tag{25}$$

for the decay of magnetization governed by the ST regime. Spins governed by the MAV regime are taken to be included

in the distribution $h(T_2)$ because their relaxation cannot be separated into diffusive and surface relaxation components [5]. Strictly we should recognize that pores with characteristic length scales $\ell_s > \ell_*$ and $\ell_s < \ell_*$ should be treated separately. This so-called local gradient approximation (LGA) fails outside of the ST regime [49]. Where the pore size distribution spans the critical length ℓ_*, we should model the decay by

$$\frac{M(t,t_E)}{M_0} \simeq \int dT_2 h_{ST}(T_2) \int_0^{g_{max}} dg_{eff} f(g_{eff}) \times \exp\left(-\frac{1}{12} D_0 \gamma^2 g_{eff}^2 t_E^2 t\right) \exp\left(-\frac{t}{T_2}\right) + \int dT_{2,eff} h_{MAV}(T_{2,eff}) \exp\left(-\frac{t}{T_{2,eff}}\right), \quad (26)$$

which, as $t_E \to 0$, reduces to

$$\frac{M(t,0)}{M_0} \simeq \int dT_2 h_{ST}(T_2) \exp\left(-\frac{t}{T_2}\right) + \int dT_{2,eff} h_{MAV}(T_{2,eff}) \exp\left(-\frac{t}{T_{2,eff}}\right). \quad (27)$$

Here, we define the terms for the ST and MAV regimes separately. In an earlier publication [5] these terms were combined and only the ST exponent (which varies as $t_E^2 t$) was given on the basis that, even when all the terms are defined explicitly as in Eq. (26), the ST exponent is still only an approximation for the magnetization decay [53].

In summary, we define the diffusion regimes expected to be observable in an arbitrary three-dimensional pore.

(a) The short-time (ST) regime occurs when $\ell_E \ll \ell_s, \ell_g$. The echo time defines the diffusive length scale observed. The magnetization decay will be a sum of diffusive attenuation and surface relaxation contributions and will be characterized by a τ^3 dependence. This regime can be observed theoretically for any sample if a short enough echo time can be employed.

(b) The Motional Averaging (MAV) regime occurs when $\ell_s \ll \ell_g, \ell_E$. The pore size defines the maximum diffusion distance. The magnetization decay will be determined predominantly by surface relaxation, pore size, and diffusion rate, characterized by a τ dependence. This regime will be observed typically in small pores with weak internal gradients.

(c) The localization regime occurs when $\ell_g \ll \ell_s, \ell_E$. The magnetic field profile across the pore determines predominantly the magnetization decay. Magnetization will be observed only where spins are diffusing in regions of local gradient extrema or near the pore walls. The asymptotic localization regime is unlikely to be observed experimentally, but we conjecture that a preasymptotic behavior will be seen in which the magnetization decay will exhibit an unusual τ dependence that is neither linear nor cubic. This regime will be observed typically in the presence of large internal gradients.

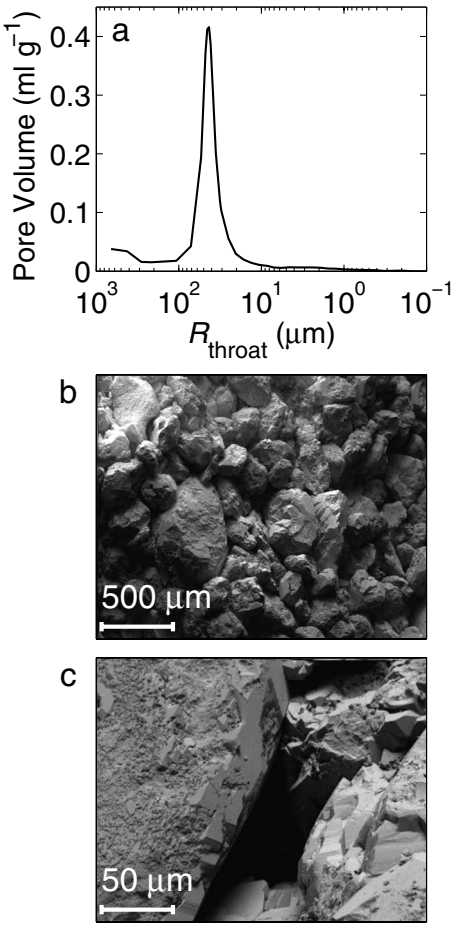

FIG. 1. (a) Mercury intrusion porosimetry data for the Benthemier sandstone reveals a monodispersed pore throat size distribution with a modal pore throat diameter of $\langle R_{throat} \rangle = 43$ μm and FWHM $\Delta R_{throat} \approx 30$ μm; SEM images (b) and (c) indicate the sandstone has a regular grain-pack structure. A typical large intergranular pore is visible in the center of (c).

III. MATERIALS

All the experiments in this paper were conducted on Bentheimer sandstone rock saturated with 2 wt. % KCl brine to prevent osmotic swelling of the clay content. The cores studied were of diameter 25 mm and length 60 mm to fit all the available NMR probes. Each of the cores was vacuum saturated and stored under brine when not in use. For the duration of the NMR experiments, the cores were wrapped in thin plastic film to prevent evaporation or excess drainage. Repeat experiments on different cores provided consistent NMR results.

To provide additional information on the rock structure, mercury intrusion porosimetry (MIP) measurements (MCA Services, U.K.) were used to determine a pore throat size distribution; see Fig. 1(a). This revealed a monomodal distribution with an average throat diameter of $\langle R_{throat} \rangle = 43$ μm, and a full width half maximum (FWHM) $\Delta R_{throat} \approx 30$ μm. Although this does not necessarily reflect the underlying pore body size distribution directly, it would suggest the rock structure is reasonably homogeneous. This conclusion is further supported by Scanning Electron Microscopy (SEM) im-

ages, Figs. 1(b) and 1(c), where the rock is seen to be composed of discrete sand grains. Large intergranular pores are visible, although there is no evidence for significant smaller intragranular porosity in this sample. Energy dispersive x-ray spectroscopy (EDX) measurements [56] confirmed the presence of small quantities of clay.

IV. NMR MEASUREMENTS AND DATA ANALYSIS

The NMR measurements were conducted using magnets with five different field strengths. The low-field permanent magnets had strengths of $B_0=42$ and 282 mT with solenoid radio frequency (rf) coils tuned to ^{1}H Larmor frequencies of $\upsilon_0=1.93$ and 12.93 MHz, respectively. The low-field measurements utilized an Oxford Instruments' Molecular Biotools Maran-DRX spectrometer. The high-field superconducting magnets had strengths of $B_0=2$, 4.7, and 9.4 T with birdcage rf coils tuned to ^{1}H Larmor frequencies of $\upsilon_0=85.18$, 199.71, and 400.23 MHz, respectively. The measurements in the 2 and 9.4 T magnets were conducted with Bruker Biospin AV spectrometers, while the measurements in the 4.7 T magnet were conducted with a Bruker Biospin DMX spectrometer. The rf pulse durations t_{90}, corresponding to a 90° tip angle, were $t_{90}=10$, 12, 15, 27, and 58 μs at the field strengths of $B_0=0.042$, 0.282, 2, 4.7, and 9.4 T, respectively. In all cases, the pulse durations corresponding to a 180° tip angle were $2t_{90}$. The long rf pulse lengths and low duty cycle tolerance of the 9.4 T system limited the minimum echo spacing in a CPMG train to $t_E=2$ ms. This limit on the echo spacing was imposed on all the systems to provide comparable data.

A. Magnetic susceptibility

The magnetic susceptibility difference between the rock and water, required to calculate the maximum effective gradient $g_{\max}$ and critical length ℓ_*, can be determined from the line broadening caused by the heterogeneous material [20]. To determine this, a water phantom of equal dimensions to the rock core was placed in the rf coil and the B_0 field well shimmed to the phantom. The FWHM Δx_{water} of the spectral line was measured. The rock core was then substituted for the water phantom and the FWHM Δx_{rock} determined without adjusting the shim settings. Assuming the line shapes are Lorentzian, the FWHM corresponds to the condition $1/\pi T_2^*$, where T_2^* is the observed transverse relaxation due to dipolar spin interactions and fluctuations in local magnetic field such that

$$\frac{1}{T_2^*}=\frac{1}{T_2}+\gamma\Delta\chi B_0+\gamma\Delta B_0, \tag{28}$$

where ΔB_0 is the inhomogeneity inherent in the static B_0 field, determined by the physical characteristics of the NMR magnet. The line broadening $\Delta\upsilon_0$ (in Hz) is obtained by deconvolution of the spectral lines. The susceptibility difference is

$$\Delta\chi=\frac{\pi\Delta\upsilon_0}{\gamma B_0}, \tag{29}$$

neglecting a prefactor of order unity that will be determined by the geometry of the sandstone grains.

B. Internal gradients

To determine the strengths of the internal gradients the method proposed by Sun and Dunn [6] was used. If the total CPMG acquisition time $t_0=nt_E$ is kept constant while the number of echoes n (and hence echo time t_E) is varied, the intensity of the echo acquired at time t_0 will depend only on the internal gradient term in Eq. (25) [20]. The other terms in Eq. (25) are dependent on the absolute acquisition time t_0 and therefore will not change as the echo time varies. Here, the echo times were varied logarithmically in 32 steps and spanned echo times of $t_E^{(1)}=2$ ms to $t_E^{(32)}=20$ ms. If t_0 is sufficiently short such that $\ell_E \ll \ell_*, \ell_s$ (the ST regime), the intensity of single echoes acquired at time t_0 will be described by

$$\frac{M(t_0,t_E)}{M(0)}=\sum_i h(T_2)\exp\left(-\frac{t_0}{T_{2,i}}\right)\times\int_0^{g_{\max}} f(g_{\text{eff}})\exp\left(-\frac{1}{12}\gamma^2 g_{\text{eff}}^2 D_0 t_E^2 t_0\right)\mathrm{d}g_{\text{eff}}. \tag{30}$$

The first summation term in T_2 can be treated as a constant for fixed t_0 and the resultant function can be fitted as a distribution of exponential diffusive decays. For this analysis, the one-dimensional Fredholm integral was inverted using Tikhonov regularization with the optimization parameter chosen by the Generalized Cross Validation (GCV) method [57,58].

C. T_1 and T_2 measurements

Longitudinal T_1 relaxation times were determined using the conventional inversion recovery pulse sequence [59]: a 180° rf inversion pulse is followed by a variable recovery delay T_{RD}, after which a 90° rf excitation pulse is used to interrogate the degree of recovery of the spin ensemble. In all cases, the recovery delays were spaced logarithmically and spanned $T_{RD}=500$ μs to 10 s in 32 steps.

Transverse T_2 relaxation times were determined using the conventional CPMG pulse sequence [22,23] with variable echo spacing. Typically, the number of echoes was varied so as to maintain a total observation time of $t_0\sim 5$ s. Echo spacings of $t_E=2$, 4, 10, 20, and 40 ms were used, corresponding to diffusive path lengths of $l_E\approx 2.14$, 3.03, 4.80, 6.78, and 9.59 μm, respectively. A $NiCl_2$ solution was used as a calibration sample to allow the T_1 and T_2 data to be scaled to an approximately consistent value of M_0 across all the magnets.

Both T_1 and T_2 relaxation time data are characterized by sums of exponentials and therefore have corresponding one-dimensional Fredholm integrals. These integrals were in-

verted using Tikhonov regularization with GCV optimization.

D. T_2-T_2 exchange measurements

The T_2-T_2 (REXSY) relaxation exchange measurement [28,29] consists of two CPMG echo trains containing m and n echoes, respectively, separated by a storage interval t_S. In all cases the echoes are separated by a constant echo time t_E=2 ms. The first CPMG echo train allows the spins to dephase with $T^A_{2,\mathrm{eff}}$ across a variable time t_A; the length of this echo train is adjusted by incrementing m in successive experiments. The number of m echoes was varied logarithmically in 32 increments from m=2 to 1024. The spins are then stored alternately on the $\pm z$ axis to be recovered as a stimulated echo [24]. The storage intervals were t_S=50, 500, and 1000 ms. Additional exchange measurements were made at v_0=400 MHz with storage times ranging from t_S=5 ms to 2 s. During the storage interval a homospoil gradient of amplitude $G_{x,y,z}$=5 G cm^{-1} is applied on all three gradient axes for 4 ms to remove any coherent spins remaining in the x-y plane. At the end of the storage interval the spins are recovered and the complex intensity of each echo in the second CPMG train of fixed duration t_B (n=1024) recorded. Each echo decay in the two-dimensional data set is phase rotated and the resulting real data are inverted numerically to provide a correlation map of $T^A_{2,\mathrm{eff}}$ against $T^B_{2,\mathrm{eff}}$.

E. Two-dimensional inversion algorithm

The two-dimensional T_2-T_2 data sets were inverted using MATLAB code based on the method described by Venkataramanan *et al.* [31]. The acquired signal will be described by a Fredholm integral of the first kind with the tensor product structure

$$M(t_A,t_B) = \int\int k_1(x,t_A)k_2(y,t_B)\mathcal{F}(x,y)\mathrm{d}x\mathrm{d}y + \epsilon(t_A,t_B), \tag{31}$$

where k_1 and k_2 are exponential kernel functions and ϵ is the experimental noise. In the case of the T_2-T_2 experiment, both kernels have the form

$$k_{1,2} = \exp\left\{-\frac{t_{A,B}}{T^{A,B}_{2,\mathrm{eff}}}\right\}, \tag{32}$$

where A and B denote the two dimensions of the experiment. In matrix notation, Eq. (31) becomes $M=K_1FK_2^{\mathrm{T}}+E$, where $^{\mathrm{T}}$ denotes the transpose of the matrix. The optimum solution for the inverse problem can be found from

$$\min\|\tilde{M} - K_1FK_2^{\mathrm{T}}\|^2 + \alpha\|F\|^2, \tag{33}$$

where $\|\ldots\|^2$ is the Frobenius norm of a matrix, α is the Tikhonov regularization smoothing parameter, and $\tilde{M} = U_1^{\mathrm{T}}MU_2$ is the compressed data where $U_{1,2}$ and $V_{1,2}$ are unitary matrices of the Singular Value Decomposition (SVD) of the kernel matrices determined from

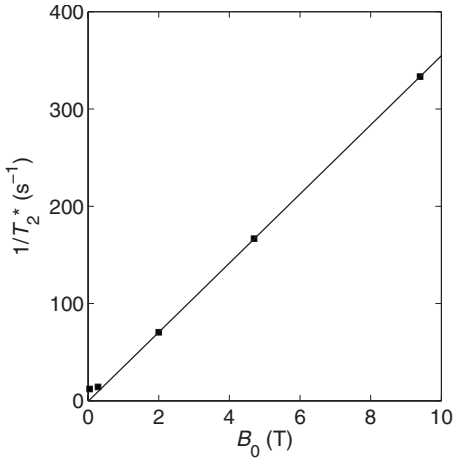

FIG. 2. Variation in transverse relaxation T_2^* as a function of magnetic field strength B_0. The straight line is a fit to the high magnetic field data points ($B_0>2$ T) and is shown as a guide to the eye. The measurements at low magnetic field strengths deviate from this line due to the inherent ΔB_0 of the permanent magnets.

$$K_{1,2} = U_{1,2}\Sigma_{1,2}V^{\mathrm{T}}_{1,2}. \tag{34}$$

$\Sigma_{1,2}$ are diagonal matrices containing the singular values listed in decreasing order. The optimum value of α is determined using the Butler-Reeds-Dawson (BRD) method [60].

V. RESULTS AND DISCUSSION

A. Magnetic susceptibility

By examining the line broadening that occurred on placing the water saturated sandstone rock core in a range of magnetic fields, it was possible to estimate the susceptibility difference between the solid and liquid phases as being $\Delta\chi = 2\times10^{-6}$. This is smaller than an independent measure of the magnetic susceptibility contrast between the rock and brine of $\Delta\chi=(1.92\pm0.01)\times10^{-5}$ determined using a Sherwood Scientific Mk1 magnetic susceptibility balance. This particular sandstone exhibits a relatively small susceptibility contrast compared to other sandstones studied previously [5]. The value of $\Delta\chi=2\times10^{-6}$ was determined predominantly from the high-field magnet measurements ($B_0\geq2$ T) where the line broadening was significant. In the low magnetic fields ($B_0<0.3$ T), the natural line width ΔB_0 of the permanent magnets was on a similar order of magnitude to the line broadening $\Delta\chi B_0$ caused by the rock, making an accurate estimate of the susceptibility difference difficult. It has been noted elsewhere that the spectral line observed from water saturated rocks is, to a good approximation, Lorentzian [52]. Therefore, the measured T_2^* decay is a single-component exponential function. In Fig. 2, the variation of $1/T_2^*$ with field strength is shown. For the high-field magnets where $B_0\geq2$ T, $T_2^*\propto B_0^{-1}$; the magnetic field inhomogeneities defined by $\Delta\chi B_0$ are dominant over the dipolar spin interactions and dictate the relaxation mechanism. At low magnetic fields, this relation breaks down due to a reduction in both T_2 and $\Delta\chi B_0$, and an increase in the term ΔB_0. The inhomogeneity of the static magnetic field becomes significant, typically, with the use of permanent magnets.

TABLE I. Values of critical length ℓ^*, dephasing time $t_{E,\max}$, and internal gradient $g_{\max}$ that define the division between the diffusion regimes in water saturated Bentheimer sandstone, calculated for a range of field strengths B_0 using $\Delta\chi = 2\times10^{-6}$ and $D_0 = 2.3\times10^{-9}$ m^2 s^{-1}.

Spectrometer	Big-2	12 MHz	AV85	DMX200	AV400
υ_0 (MHz)	1.93	12.93	85.15	199.71	400.23
B_0 (T)	0.042	0.282	2.00	4.70	9.40
$\gamma B_0\times10^6$ (s^{-1})	12.12	75.40	534.1	1257	2513
ℓ_* (μm)	9.74	3.91	1.47	0.96	0.68
$t_{E,\max}$ (ms)	41.25	6.60	0.94	0.40	0.20
$g_{\max}$ (T m^{-1})	0.0086	0.15	2.73	9.83	27.70

B. Internal gradients

From the measured value of $\Delta\chi$, and the known values of B_0 and D_0 (bulk water), it is possible to predict the maximum echo time $t_{E,\max}\approx\ell_*^2/D_0$ for which diffusion in the MAV regime can be observed, and the maximum internal gradient $g_{\max}$ that would be present in the pores using Eqs. (18) and (19) as appropriate. The results are summarized in Table I.

Distributions of internal gradients in the water saturated sandstone rock core at different magnetic field strengths are shown in Fig. 3, and a summary of the log-mean and range of g_{eff} is shown as a function of B_0 in Fig. 4. It is seen that $g_{\max}$ scales approximately with $B_0^{3/2}$ as predicted from Eq. (18), cf. upper error limits and solid line in Fig. 4. The best agreement between the measured internal gradient distributions and the theoretical maximum gradient values from Table I are found at the intermediate field strengths [corresponding to $\upsilon_0=12$ and 85 MHz: Figs. 3(b) and 3(c), respectively] where the accessible range of t_E values fitted using Eq. (30) were appropriate for the range of g_{eff} present in the sample. At the lowest field strength, corresponding to $\upsilon_0=2$ MHz, Fig. 3(a), the internal gradients were small and so insufficient diffusive attenuation was obtained to provide a good fit. Conversely, at the highest field strengths [corresponding to $\upsilon_0=200$ and 400 MHz: Figs. 3(d) and 3(e), respectively] hardware limitations prevented short enough echo times from being employed to probe the ST regime unambiguously. Therefore, as discussed later in light of the $T_{2,\text{eff}}$ measurements, these internal gradient distributions only reflect the weakest internal gradients and so provide a lower limit for g_{eff} at high magnetic field strengths. Nevertheless, the results in Fig. 4 confirm the expected trend in internal gradient with magnetic field strength, and provide good agreement with the predicted maximum internal gradients. Furthermore, both log-mean g_{eff} and $g_{\max}$ increase more strongly than the hypothetical B_0 scaling (dashed line in Fig. 4) expected from magnetostatic arguments without regard to diffusion.

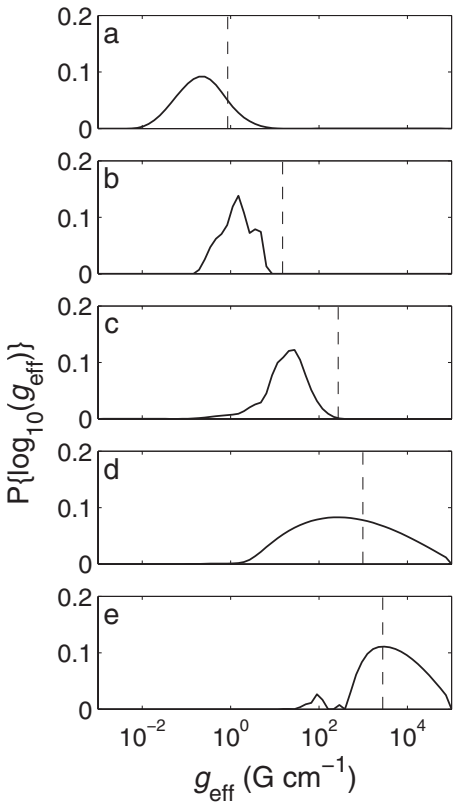

FIG. 3. Probability distributions of internal gradients g_{eff} present in a water saturated sandstone rock core at (a) $\upsilon_0=2$, (b) 12, (c) 85, (d) 200, and (e) 400 MHz, normalized to unit area. The theoretical maximum internal gradients $g_{\max}$ (from Table I) are indicated by the vertical dashed lines.

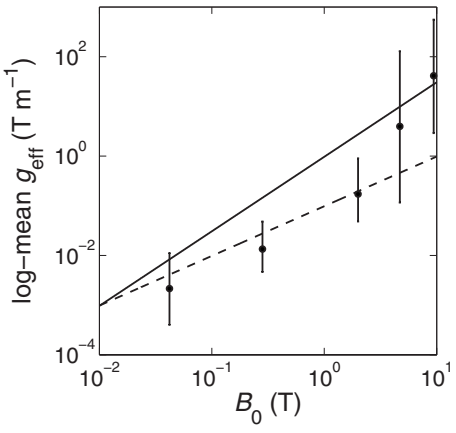

FIG. 4. Variation in average internal gradient log-mean g_{eff} as a function of magnetic field strength B_0. Overall ranges of g_{eff} are indicated by the error bars. The maximum theoretical internal gradient $g_{\max}$ is indicated by the solid line, determined from Eq. (19) and has a power law dependence of 3/2. A hypothetical $g_{\max}$ with a power law dependence of 1 (dashed line) is shown for comparison.

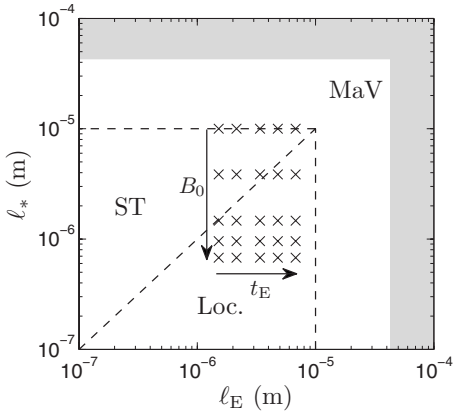

FIG. 5. Schematic representation of regimes for molecular diffusion in pores. Experimental CPMG data were collected at the points indicated (×). Approximate boundaries between the ST, localization, and MAV regimes are indicated by dashed lines. These boundaries are blurred, and close to the boundaries, intermediate diffusion behavior will be observed. The minimum ℓ_s, i.e., the boundary defining the MAV regime, has been taken as $R_{\min} \approx 10$ μm from Fig. 1. The shaded area indicates $\ell_s > \langle R_{\text{throat}} \rangle$, a better indicator, potentially, of the experimental conditions necessary to observe motional averaging in this rock.

By calculating the values of ℓ_* and ℓ_E defined by the experimental parameters, and obtaining an estimate of $\ell_s \sim \langle R_{\text{throat}} \rangle$ from Fig. 1(a), it is possible to estimate the diffusion regimes in which the $T_{2,\text{eff}}$ measurements are expected to occur. A plot of ℓ_* against ℓ_E is given in Fig. 5, assuming a uniform magnetic field gradient exists within individual pores. The diffusive length scales probed by the parameters in the $T_{2,\text{eff}}$ experiments discussed in this work are identified (×). The schematic implies that the edges of these regimes are well-defined (dashed lines); in a real system this is not true and measurements near these edges will probe regimes of intermediate diffusion behavior. At low magnetic field strength and short echo times, the measurements should be in the ST regime, and approach the MAV regime for the smallest pores. As the field strength and echo time increase, the measurements shift into the localization regime. For the high-field measurements (corresponding to $v_0 = 200$ and 400 MHz, even the data acquired at the shortest echo times exhibit $\ell_* < \ell_E$. This confirms that at high magnetic field strengths, it will not always be possible to obtain an echo time short enough to probe the ST regime.

It is important to note that the magnetic field gradients in the pores studied here are likely to be nonuniform, as discussed in Sec. II. Based on this theory, it is reasonable to conclude that the boundaries of the diffusion regimes laid out in Fig. 5 will be inadequate to define the diffusion behavior observed in this work. Notwithstanding, it is reasonable to assume from Fig. 5 that the $T_{2,\text{eff}}$ measurements conducted at the high magnetic field strengths (corresponding to $v_0 = 200$ and 400 MHz) will exhibit the characteristic properties of diffusion in a bounded magnetic field profile governed by the preasymptotic localization regime, specifically: (i) magnetization that varies on a length scale less than the pore size, (ii) sensitivity to the internal gradients, and (iii) only a weak dependence on surface relaxation. Figure 5 suggests that only the low-field measurements (corresponding to $v_0 = 2$ MHz) will be in the ST regime.

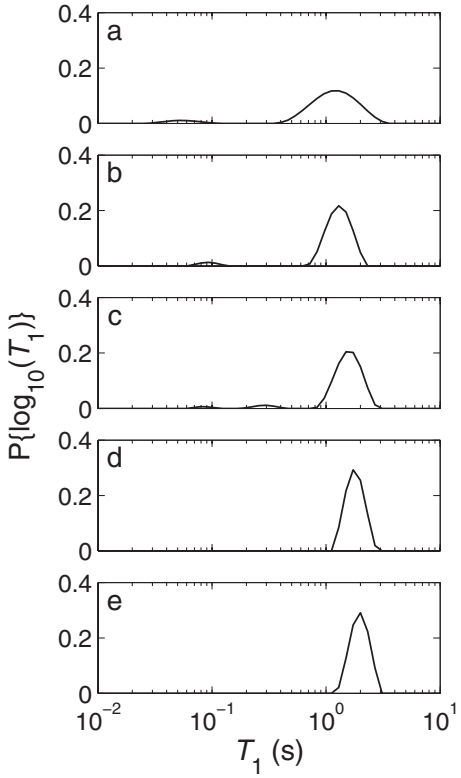

FIG. 6. Probability distributions of T_1 relaxation times determined for a water saturated sandstone rock core at (a) $v_0 = 2$, (b) 12, (c) 85, (d) 200, and (e) 400 MHz, normalized to unit area. As B_0 increases, there is a slight increase in the log-mean T_1 and a narrowing of the T_1 distribution consistent with surface relaxation theory as discussed in the text.

C. Longitudinal relaxation

It is important to characterize the T_1 relaxation time distribution since longitudinal relaxation occurs during the storage interval in the T_2-T_2 exchange measurement. A measure of T_1 is required if exchange rates are to be determined from the data [28,29]. It has been shown previously that T_1 is independent of internal gradient strength [20] although it is weakly dependent on B_0 [19]. The T_1 distributions for the water saturated sandstone rock core are shown in Fig. 6.

As the field strength was increased, the observed mean T_1 also increased from $\langle T_1 \rangle = 1.2$ s at $v_0 = 2$ MHz, Fig. 6(a), to $\langle T_1 \rangle = 2$ s at $v_0 = 400$ MHz, Fig. 6(e). At the lower field strengths, Figs. 6(a)–6(c), some small signal component is observed at shorter T_1 times; this is attributed to water in contact with the clay components in the rock. The distribution of T_1 times narrows as B_0 increases. This is consistent with surface relaxation theory: the observed, frequency dependent relaxation rate $1/T_1$ is given by the sum of the bulk relaxation rate $1/T_{1,\text{bulk}}$ and surface relaxation rate $1/T_{1,\text{surf}}$ such that

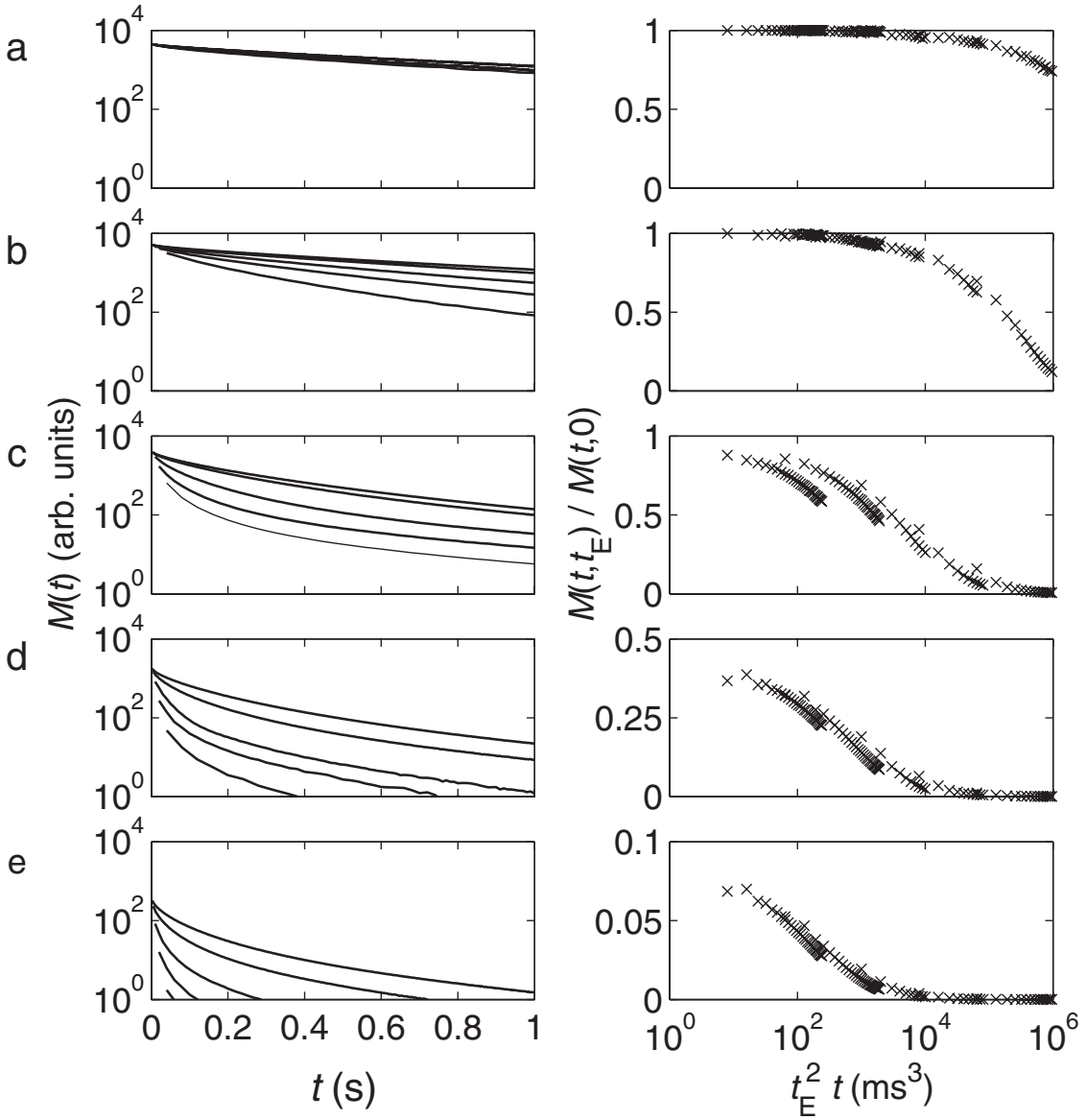

FIG. 7. Observed magnetization decays using CPMG determined for a water saturated sandstone rock core at (a) v_0=2, (b) 12, (c) 85, (d) 200, and (e) 400 MHz. The same data is shown twice: (left) the signal amplitudes have been calibrated such that $M_0=5\times10^3$ units in each plot and the vertical scale has been truncated at the noise floor of the data in (e); (right) the signal amplitudes have been normalized with respect to a "gradient-free" CPMG decay (approximated by data acquired with t_E=200 μs at v_0=2 MHz) and plotted as a function of $t_E^2 t$. In each plot, data from five decay curves with echo times of (top to bottom) t_E=2, 4, 10, 20, and 40 ms have been overlaid.

$$\frac{1}{T_1(\omega_0)} = \frac{1}{T_{1,\text{bulk}}(\omega_0)} + \frac{N_S}{N}\frac{1}{T_{1,\text{surf}}(\omega_0)}, \tag{35}$$

where N_S/N is the number ratio of surface to bulk water molecules. For a fixed temperature, Eq. (35) can be approximated by [61]

$$\frac{1}{T_1(\omega_0)} \simeq \frac{1}{T_{1,\text{bulk}}(\omega_0)} + \frac{N_S}{N}\mathcal{K}_1\tau_m \ln\left[\frac{1+\omega_0^2\tau_m^2}{\left(\frac{\tau_m}{\tau_s}\right)^2+\omega_0^2\tau_m^2}\right], \tag{36}$$

where $\mathcal{K}_1$ is constant for a given sample, τ_m is a correlation time of surface diffusion, and τ_s is the surface residency time ($\tau_m \ll \tau_s$). As ω_0 becomes large, the term in square brackets tends to unity and so, due to the logarithmic scaling, the surface relaxation becomes negligible compared to the bulk relaxation.

D. Transverse relaxation

The CPMG decays obtained from the water saturated rock core across a range of B_0 and t_E values are shown in Fig. 7. At low field, corresponding to v_0=2 MHz, Fig. 7(a) (left), there is little variation in the CPMG decays across the large span of echo times from t_E=2 to 40 ms. Here, $\ell_E < \ell_*$ in all cases so the CPMG echo time defines the diffusive path length and the magnetization decay is governed predominantly by the ST regime. However, $\ell_E \to \ell_s$ for the smallest

pore throats, so intermediate diffusion behavior between the ST and MAV regimes may apply. However, for larger pores ($R \geq \langle R_{\text{throat}} \rangle$) the condition $\ell_E \ll \ell_s$ applies. From Table I, we see that the maximum theoretical internal gradient $g_{\max} < 1$ G cm^{-1}, and therefore we observe CPMG decays that are only weakly diffusion attenuated even in the ST regime. In Fig. 7(a) (right), we see good data collapse (i.e., the data points overlap and form a continuous line) indicative of the τ^3 dependence expected in the ST regime. This is in agreement with similar low-field data published elsewhere [5].

At $v_0=12$ MHz, Fig. 7(b) (left), $g_{\max}=15$ G cm^{-1} so the degree of diffusive attenuation in the CPMG decays should be greater than at $v_0=2$ MHz; this is as expected. The first two CPMG decays overlay reasonably well and show little variation in the degree of diffusive attenuation; similarly, data collapse is observed for these CPMG data, Fig. 7(b) (right). Here, $\ell_E < \ell_*$ so the CPMG echo time defines the diffusive path length. Beyond $t_E=4$ ms, $\ell_E \geq \ell_*$; ℓ_* therefore defines the diffusion path length and the diffusion behavior is expected to be governed by the preasymptotic localization regime. Overall, the CPMG decays are seen to become increasingly divergent as the echo time increases. This is confirmed in the data collapse, Fig. 7(b) (right), where a slight deviation from a smooth line is observed in the data points at $t_E^2 t \sim 10^5$ ms^3.

At the higher field strengths, Figs. 7(c)–7(e) (left), where $g_{\max} > 100$ G cm^{-1}, the measured CPMG decay curves reflect a distribution of $T_{2,\text{eff}}$ relaxation times that is diffusion dominated: as the echo time increases the decay becomes more rapid. It is also notable that the number of exponential components in the decays increases: this is observed as a shift from near-linear decays on the log-linear plot, see Figs. 7(a) and 7(b) (left), to significantly nonlinear decays in Figs. 7(c)–7(e) (left). At the higher field strengths, corresponding to $v_0 \geq 85$ MHz, $\ell_* \leq \ell_E$ in all cases. This means ℓ_* defines the observable diffusion path length; the preasymptotic localization regime should apply. The strong dependence on internal gradient strength is clearly visible as expected.

A more significant variation in the high-field data is observed in Figs. 7(c)–7(e) (right): at $v_0=85$ MHz, the data collapse fails entirely, indicating the magnetization decay no longer depends on τ^3. This is as expected, since the CPMG decays acquired in an intermediate regime or the preasymptotic regime will have an unusual τ dependence. However, as the magnetic field strength increases, the data collapse is at least partially restored. This suggests the observed magnetization decays are similar to free diffusion in strong magnetic field gradients, and the observed magnetization decay in the preasymptotic localization regime is akin to that for the ST regime as discussed in [25], at least for the surviving magnetization.

To examine the relaxation behavior in more detail, selected decay curves from Fig. 7 (left) have been inverted to form the $T_{2,\text{eff}}$ relaxation time distributions shown in Fig. 8. At the lowest field strength, corresponding to $v_0=2$ MHz, the $T_{2,\text{eff}}$ relaxation time distributions in Fig. 8(a) have a similar shape, qualitatively, to that obtained for T_1 in Fig. 6(a): a single dominant component is observed at long $T_{2,\text{eff}}$ times with some smaller features present at shorter $T_{2,\text{eff}}$ times. At this field strength, a two-dimensional T_1-T_2 correlation (not shown) reveals the characteristic [19] ratio $T_1/T_{2,\text{eff}} \approx 1.5$ at all positions on the $T_{2,\text{eff}}$ axis [62]. As the echo time is increased, there is a slight decrease in $T_{2,\text{eff}}$ due to diffusive attenuation. A similar variation in $T_{2,\text{eff}}$ as a function of echo time was observed elsewhere for a water saturated sandstone in a low-field magnet [63]. The predominantly monomodal $T_{2,\text{eff}}$ distribution appears to be a reasonable reflection of the pore size distribution in this sample.

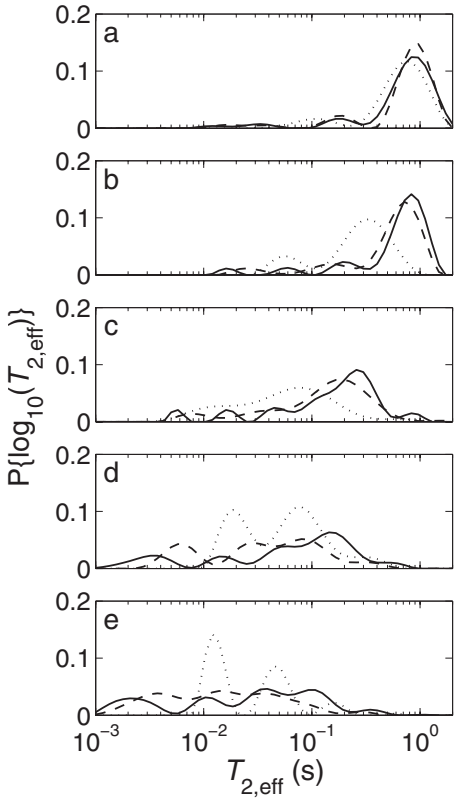

FIG. 8. Probability distributions of $T_{2,\text{eff}}$ relaxation times determined for a water saturated sandstone rock core at (a) $v_0=2$, (b) 12, (c) 85, (d) 200, and (e) 400 MHz, normalized to unit area. The individual curves correspond to echo times of $t_E=2$ ms (solid lines), 4 ms (dashed lines), and 20 ms (dotted lines) in each plot. These results were obtained by inverting the appropriate CPMG decays in Fig. 7. As B_0 increases, there is a decrease in $\langle T_{2,\text{eff}} \rangle$.

As the field strength is increased, the $T_{2,\text{eff}}$ distributions shown in Fig. 8 become complicated by an increasing number of discrete relaxation time components of similar intensity. At $v_0=400$ MHz it is possible to identify four significant, discrete relaxation time components. Elsewhere, measurements of a different water saturated sandstone at $v_0=400$ MHz also revealed four discrete $T_{2,\text{eff}}$ components [28] although this was attributed to under-smoothing in the numerical inversion (an artifact referred to as "pearling"). From Figs. 7 and 8 presented here, it is possible to conclude that the multicomponent $T_{2,\text{eff}}$ behavior observed at high-field strengths is a genuine reflection of the measured relaxation time distributions.

It is also important to note that there is considerable signal attenuation prior to the acquisition of the first echo in the CPMG decays at high magnetic field strengths, as high-

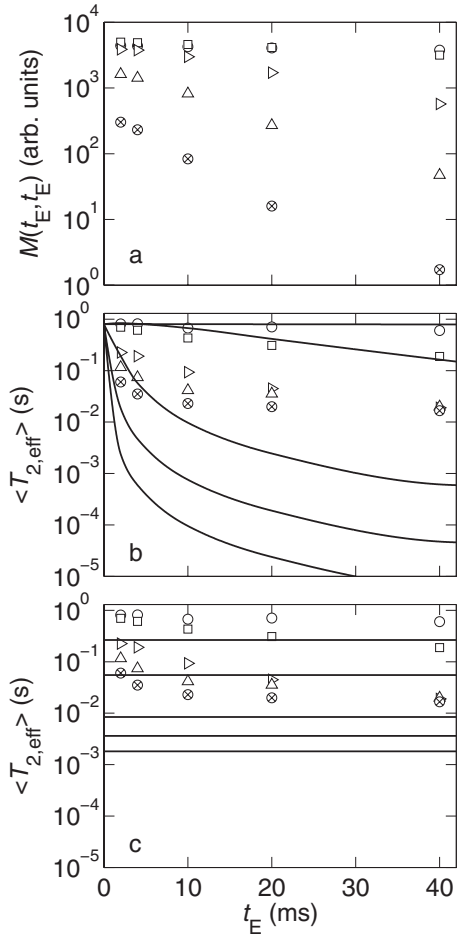

FIG. 9. (a) First echo intensities $M(t_E,t_E)$ and (b,c) log-mean transverse relaxation times $\langle T_{2,\mathrm{eff}}\rangle$ as a function of echo time t_E. These data were extracted from Figs. 7 and 8. The symbols correspond to Larmor frequencies of v_0=2 (○), 12 (□), 85 (▷), 200 (△), and 400 MHz (⊗) in each case. In (b,c) the solid lines represent analytically calculated $\langle T_{2,\mathrm{eff}}\rangle$ relaxation times at (top to bottom) v_0=2, 12, 85, 200, and 400 MHz for (b) the ST and (c) asymptotic localization regimes. These lines are obtained using Eq. (22) and Eq. (24) (with $\ell_s=\langle R_{\mathrm{throat}}\rangle$), respectively.

lighted in Fig. 9(a). For example, at v_0=400 MHz and t_E =2 ms, the first echo has an amplitude almost an order of magnitude less than $M_0=5\times10^3$. This is critical to consider since it means very short $T_{2,\mathrm{eff}}$ components are not observed, and a complete description of the $T_{2,\mathrm{eff}}$ behavior cannot be defined. Considering this significant loss of magnetization, the data collapse observed for the surviving magnetization seen in Fig. 7(e) (right), and the multiple decay modes seen in Fig. 8(e), it is reasonable to conclude that we are observing relaxation in a bounded, nonlinear magnetic field profile (hence nonuniform gradient), governed by the preasymptotic localization regime. The fact that the data collapse is restored partially at high magnetic field strengths suggests that at least some of the surviving magnetization is observed from spins experiencing a local g_{eff} that satisfies the condition for the ST regime. Yet, the presence of multiple apparent $T_{2,\mathrm{eff}}$ relaxation times in Figs. 8(d) and 8(e) suggests several distinct environments exist within the sample. These environments are likely induced by diffusion in separate regions of weak, local magnetic field gradient; this discussion is continued in Sec. V E with further supporting evidence. It is worth noting here that the restoration of the τ^3 dependence at high magnetic field strengths will mean Eq. (30) fits the data well so the derived internal gradient distributions shown in Figs. 3(d) and 3(e) appear meaningful. However, these gradient distributions will only reflect the weakest internal gradients in the sample. Higher gradients, responsible for the magnetization lost prior to the acquisition of the first echo, will not be represented in these g_{eff} distributions.

In the absence of a magnetic field gradient, T_2 relaxation time distributions should reflect the B_0 dependence seen for T_1 (Fig. 6). An expression equivalent to Eq. (36) exists for T_2 relaxation

$$\frac{1}{T_2(\omega_0)} \simeq \frac{1}{T_{2,\mathrm{bulk}}(\omega_0)} + \frac{N_S}{N}\mathcal{K}_2\tau_m\left\{2\ln\left[\frac{\tau_s}{\tau_m}\right] + \ln\left[\frac{1+\omega_0^2\tau_m^2}{\left(\frac{\tau_m}{\tau_s}\right)^2+\omega_0^2\tau_m^2}\right]\right\}. \tag{37}$$

Therefore, we would expect the observed T_2 relaxation time to tend to the T_2 value for bulk water minus an offset determined by $\ln[\tau_s/\tau_m]$ as B_0 increases. However, it is obvious from Figs. 8(a)–8(e) that as the field strength increases, $\langle T_{2,\mathrm{eff}}\rangle$ decreases, as summarized in Figs. 9(b) and 9(c). This indicates that the observed $T_{2,\mathrm{eff}}$ behavior is not governed by surface interactions and that diffusion is the dominant relaxation mechanism.

It is possible to estimate the mean $\langle T_{2,\mathrm{eff}}\rangle$ relaxation times expected for the different diffusion regimes. The observed and expected $\langle T_{2,\mathrm{eff}}\rangle$ relaxation times for the ST regime as a function of t_E are compared in Fig. 9(b). The results deviate when a significant portion of the $T_{2,\mathrm{eff}}$ distribution contains relaxation times of $T_{2,\mathrm{eff}} \ll t_E$. This discrepancy provides further evidence that the internal gradient distributions in Figs. 3(d) and 3(e) fail to represent the full range of gradient strengths in the sample. In these cases the exponential components associated with the short relaxation time modes are not observed; this is obvious from Fig. 9(a) where, at large B_0 and t_E, a significant fraction of the signal has been lost prior to the acquisition of the first echo intensity. The deviation between the simulated and observed $\langle T_{2,\mathrm{eff}}\rangle$ in the ST case provides an indication of the point at which the $T_{2,\mathrm{eff}}$ distribution will no longer reflect the pore size distribution.

The observed and expected $\langle T_{2,\mathrm{eff}}\rangle$ relaxation times for the asymptotic localization regime are compared in Fig. 9(c). In all cases the expected echo time independent values are lower than those observed by an order of magnitude, typically. This confirms that the apparent progression of $\langle T_{2,\mathrm{eff}}\rangle$ to a constant value at high magnetic field strengths and long echo times is an artifact of the measurement (due to the loss of short $T_{2,\mathrm{eff}}$ components), rather than magnetization decay in the asymptotic localization regime.

For completeness, we state that the expected $\langle T_{2,\mathrm{eff}}\rangle$ times for the MAV regime (not shown) are orders of magnitude lower than the observed $\langle T_{2,\mathrm{eff}}\rangle$ times in Fig. 9(b) and 9(c)

due to the R^2 scaling in Eq. (23) for these "large" pores.

From Fig. 9, it is possible to conclude that the $\langle T_{2,\mathrm{eff}}\rangle$ times can be approximated by free diffusion in the effective gradients at low magnetic field strengths. As such, it is possible to define a guideline to assess whether the measured $T_{2,\mathrm{eff}}$ relaxation time distribution of a given system under the condition of ST diffusion will reflect the pore size distribution. This is determined from the average internal gradient $\langle g_{\mathrm{eff}}\rangle$, the echo time t_E, and the observed average relaxation time $\langle T_{2,\mathrm{eff}}\rangle$. From Eq. (22), it is possible to say that if

$$\langle T_{2,\mathrm{eff}}\rangle < \frac{12}{D_0\gamma^2\langle g_{\mathrm{eff}}\rangle^2 t_E^2}, \tag{38}$$

the observed $T_{2,\mathrm{eff}}$ relaxation time distribution will reflect the pore size distribution. This is related to the criterion [5]

$$\frac{1}{12}D_0\gamma^2 g_{\max}^2 t_E^2 t < 1, \tag{39}$$

for observing negligible diffusive decay in a CPMG echo train. From Fig. 9(b), we can see that the limit in Eq. (38) is exceeded at a field strength of $B_0=2$ T (corresponding to $\upsilon_0=85$ MHz) and an echo time $t_E>2$ ms, beyond which the simulated $\langle T_{2,\mathrm{eff}}\rangle$ relaxation time deviates rapidly from the observed value. Good agreement between the observed and analytically determined $\langle T_{2,\mathrm{eff}}\rangle$ times are seen at the lower field strengths. For this water saturated sandstone sample and the range of echo times employed, the maximum Larmor frequency that could be used to produce $T_{2,\mathrm{eff}}$ distributions that are representative of the pore size distribution is estimated at $\upsilon_0=15$ MHz. However, in practice, it is unlikely that anyone would measure a CPMG decay with $t_E=40$ ms (it is usual to minimize the echo time within the limits of the hardware) although such echo times are used in measurements of diffusion and advection [41]. Therefore, higher magnetic field strengths can be employed in CPMG-like $T_{2,\mathrm{eff}}$ analysis as long as t_E remains sufficiently short to ensure $\ell_E \ll \ell_*$.

E. Relaxation exchange

So far we have explored the dependence of $T_{2,\mathrm{eff}}$ on magnetic field strength. Here, we extend this to the two-dimensional T_2-T_2 relaxation exchange measurement. From the SEM images in Fig. 1 an average sand grain radius of ~ 100 μm can be estimated. It is therefore reasonable to assume that diffusive exchange between intergranular porosity will occur on the time scale of several seconds. Exchange is observed in T_2-T_2 plots by the evolution of peaks placed symmetrically either side of the diagonal where $T_{2,\mathrm{eff}}^A = T_{2,\mathrm{eff}}^B$ [27]. At $\upsilon_0=2$ MHz, Fig. 10(a), there is no sign of exchange. At a storage time of $t_S=50$ ms the projections onto the $T_{2,\mathrm{eff}}^A$ and $T_{2,\mathrm{eff}}^B$ axes (not shown) look similar to the one-dimensional $T_{2,\mathrm{eff}}$ distribution in Fig. 8(a) (solid line). As the storage time increases up to $t_S=1$ s the shorter $T_{2,\mathrm{eff}}$ components disappear due to T_1 relaxation although there is still no sign of exchange.

As the magnetic field strength is increased so that $\upsilon_0=12$ MHz, Fig. 10(b), low intensity peaks are visible on opposite sides of the $T_{2,\mathrm{eff}}^A = T_{2,\mathrm{eff}}^B$ diagonal. These increase slightly in intensity as the storage time increases, suggesting the presence of two distinct magnetization reservoirs between which spins are exchanging on the time scale of experiment.

At higher field strengths, Figs. 10(c)–10(e), more relaxation time components are observed and the two-dimensional plots become difficult to interpret. For example, at $\upsilon_0=400$ MHz, Fig. 10(e), it is possible to discern four discrete relaxation components on the $T_{2,\mathrm{eff}}^A = T_{2,\mathrm{eff}}^B$ diagonal. Exchange is observed between each of these components, identified as A–D in Fig. 11(a) that shows the one-dimensional projection along the $T_{2,\mathrm{eff}}^A = T_{2,\mathrm{eff}}^B$ axis taken from a T_2-T_2 distribution with $t_S=5$ ms (not shown). This projection differs slightly from the one-dimensional data in Fig. 8 due to the different inversion algorithm employed. These four discrete $T_{2,\mathrm{eff}}$ components result in a total of six exchange pathways. By integrating the peaks in the two-dimensional plots associated with each of the exchange pathways, the exchange peak intensities I_{XP} can be determined, see Fig. 11(b). Error bars are shown on some data points, determined by adding additional random noise to the data with a standard deviation equivalent to that of the experimental noise, and repeating the inversion [29]. These exchange peak intensities are normalized using the total peak intensity I_{TP} to account for the varying signal loss due to longitudinal relaxation. I_{XP}/I_{TP} can be fitted with a single-component exponential recovery [28]

$$\frac{I_{XP}(t_S)}{I_{TP}(t_S)} = \frac{I_{XP}(t_{S,\infty})}{I_{TP}(t_{S,\infty})}\left[1-\exp\left(-\frac{t_S}{\kappa_{\mathrm{eff}}}\right)\right], \tag{40}$$

to estimate an effective exchange time κ_{eff}, where $t_{S,\infty}$ is the final storage time in the experiment. Since there is only a single T_1 relaxation time component for this sample at $\upsilon_0=400$ MHz, the measured effective exchange time κ_{eff} is corrected according to [28]

$$\frac{1}{\kappa} = \frac{1}{T_1} + \frac{1}{\kappa_{\mathrm{eff}}}, \tag{41}$$

to obtain a better estimate of the exchange time τ. The least-square fits of Eq. (40) to the data are shown in Fig. 11(b) (solid lines) and the extracted exchange times for each of the exchange pathways are summarized in Table II. A corresponding exchange distance R_X can be calculated using the Einstein equation for three-dimensional diffusion

$$R_X = \sqrt{6D_0\kappa}. \tag{42}$$

Elsewhere, a more complete model for exchange has been presented [29]. In order to extract exchange times from this model, further knowledge of the spin system is required (e.g., T_1, $T_{2,\mathrm{eff}}$, and initial magnetization of each reservoir, independent of exchange) and these parameters are difficult to determine accurately in this case.

The estimated exchange distances given in Table II are similar to those determined elsewhere for a different water saturated sandstone rock measured at $\upsilon_0=400$ MHz [28]. Exchange is seen to occur here between all four discrete relaxation environments. The exchange distance between

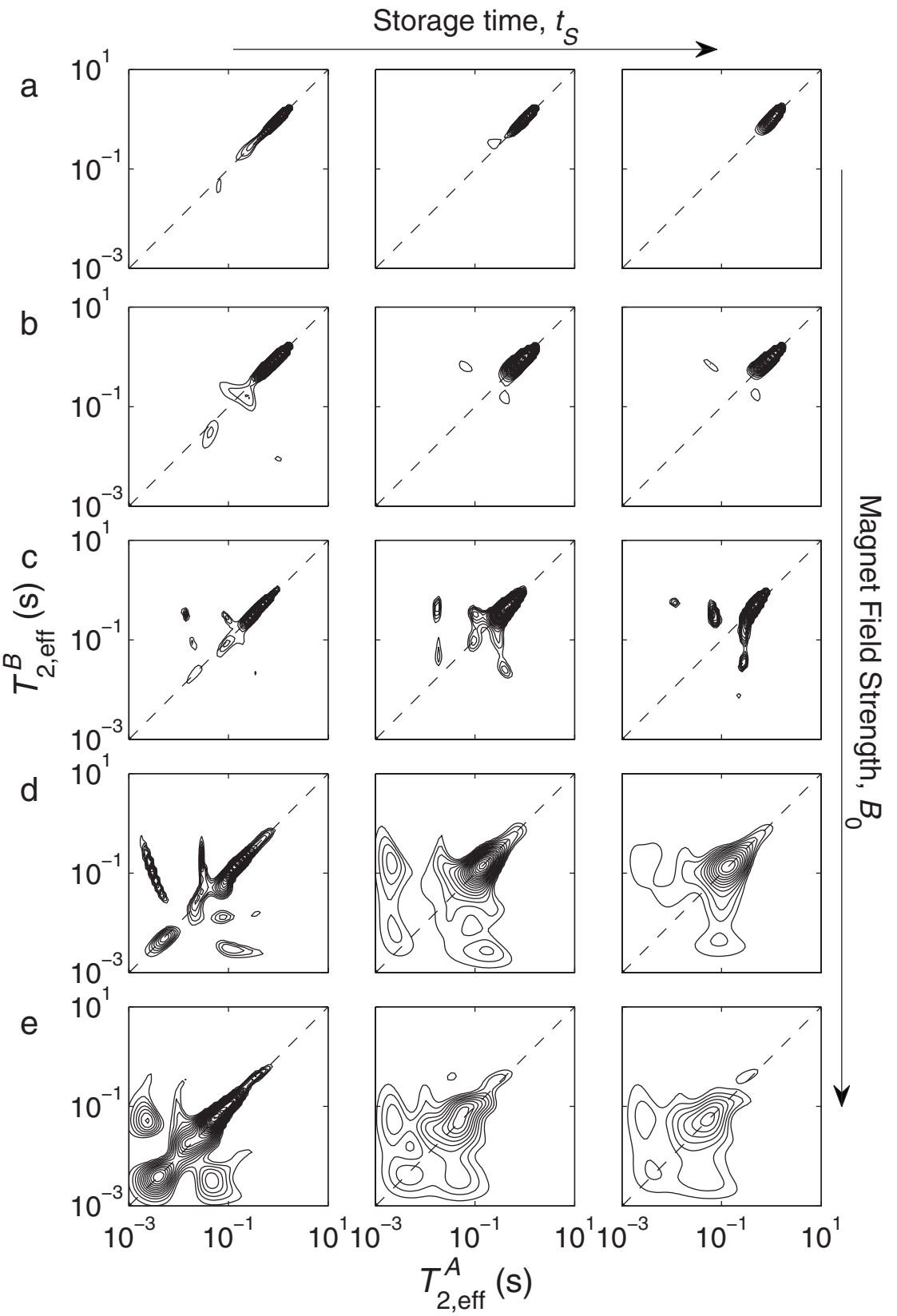

FIG. 10. A selection of T_2-T_2 relaxation correlation plots determined for a water saturated sandstone rock core at (a) v_0=2, (b) 12, (c) 85, (d) 200, and (e) 400 MHz. In each case, the storage times were (left to right) t_S=50, 500, and 1000 ms. The dashed diagonal lines indicate $T^A_{2,\mathrm{eff}}=T^B_{2,\mathrm{eff}}$. The contour intervals are the same in each plot; the intensity of the plots decreases as t_S increases due to T_1 relaxation during the storage interval. As B_0 increases, the two-dimensional plots become more complicated and exhibit a greater number of discrete relaxation components between which diffusive exchange is observed.

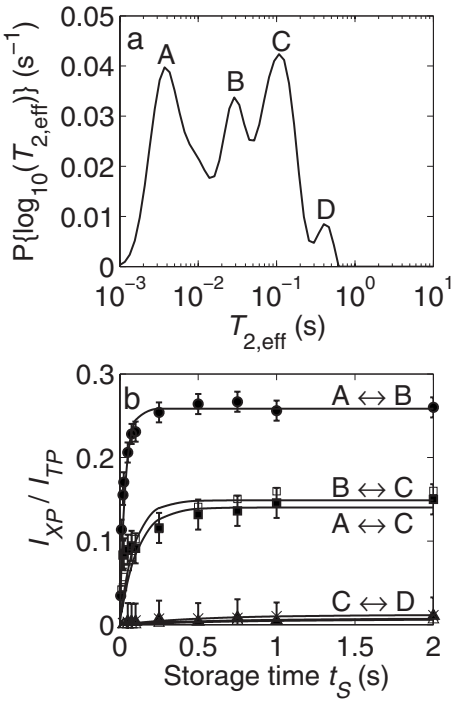

FIG. 11. (a) $T_{2,\mathrm{eff}}$ probability distribution, normalized to unit area, extracted from a T_2-T_2 plot obtained for a water saturated sandstone rock core at υ_0=400 MHz with a storage time of t_S =5 ms. Four $T_{2,\mathrm{eff}}$ components can be identified, labeled A–D, respectively. (b) Normalized exchange peak intensity I_{XP}/I_{TP} plotted as a function of storage time for each of the exchange pathways between the discrete magnetization reservoirs: A↔B (●), A↔C (■), B↔C (□), A↔D (▲), B↔D (△), and C↔D (×). Example error bars are shown on the data with solid symbols (see text for details). The lines are monoexponential fits to the data as indicated by the labels. The fits to the data for the pathways A↔D and B↔D have very low intensity and are visible below the fit to the C↔D data.

$T_{2,\mathrm{eff}}$ components A, B, and C are on the order of R_X ~32 μm, consistent with the typical pore throat radii estimated from Fig. 1. The larger exchange distances seen between D and the other components are on the order of R_X ~82 μm, comparable to either typical pore throat diameters or the expected upper limit of the pore radii; however, the errors associated with these exchange distances make interpretation of these results ambiguous. Notwithstanding, the overall spread of the exchange distances (R_X=20–90 μm) is in agreement with the expected range of pore sizes. If the exchange peaks observed at the lower field strengths are analyzed, similar exchange distances are also estimated, with R_X~30–60 μm typically. Obviously, the number of discrete exchange pathways decreases with a reduction in B_0. At υ_0 =12 MHz (the lowest magnetic field strength at which exchange is observed), a single exchange pathway exists with R_X=50 μm ± 10 μm.

TABLE II. Summary of estimated exchange path lengths between relaxation environments A–D as identified in Fig. 11(a), observed in a water saturated sandstone rock core at υ_0=400 MHz.

Exchange path	κ_{eff} (s)	κ (s)	R_X (μm)
A↔B	0.03 ± 0.01	0.03 ± 0.01	22 ± 4
A↔C	0.11 ± 0.03	0.10 ± 0.03	38 ± 5
B↔C	0.09 ± 0.05	0.09 ± 0.05	35 ± 9
A↔D	0.63 ± 0.35	0.47 ± 0.23	81 ± 23
B↔D	0.80 ± 0.40	0.57 ± 0.24	89 ± 22
C↔D	0.52 ± 0.38	0.42 ± 0.29	75 ± 33

It is important to realize that, without due consideration to the complexities of the system under observation, the data in Table II could be interpreted in terms of pore-to-pore diffusive exchange. However, it is necessary to consider the origin of the discrete magnetization reservoirs between which the exchange occurs. The Brownstein and Tarr theory [16] states that the four reservoirs correspond to four discrete pore sizes (assuming "fast" diffusion). The combined MIP and SEM data (Fig. 1), and the low-field T_1 and $T_{2,\mathrm{eff}}$ measurements [Figs. 6(a) and 8(a), respectively], indicate a dominant monomodal pore size distribution: this pore size distribution alone would not provide the discrete relaxation time components required to observe exchange; hence no exchange peaks are visible in the T_2-T_2 measurements at υ_0=2 MHz, Fig. 10(a).

Considering the one-dimensional CPMG data presented in Sec. V D, we conclude that the $T_{2,\mathrm{eff}}$ decays observed at high magnetic field strengths are governed by the preasymptotic localization regime. The theory of the localization regime for bounded, nonlinear magnetic field profiles predicts the presence of multiple, isolated regions of surviving coherent magnetization within individual pores. Magnetization decay is observed for spins diffusing near the pore surfaces and in isolated regions of weak magnetic field gradient [36,49]. The observed exchange distances, on the order of the pore radii, are therefore in agreement with exchange occurring between these regions of residual magnetization. This implies that while the T_2-T_2 measurement cannot determine pore-to-pore exchange in these large pore rocks, it can be used as an alternative method for estimating an average pore size, and the width of the pore size distribution.

We reiterate that four relaxation environments have been observed in independent measurements of different saturated sandstones at ν_0=400 MHz [28]. This observation suggests the $T_{2,\mathrm{eff}}$ relaxation time distribution is not a unique property of the rock but evolves rather as a result of some underlying, consistent phenomenon: namely, relaxation decay in the preasymptotic localization regime. Why more than two discrete relaxation times are observed at higher magnetic field strengths is not clear; the fact that the number of relaxation time components increases with increasing magnetic field strength may indicate the development of multiple oscillations in the magnetic field profile across individual pores. Further understanding of the preasymptotic localization regime with a three-dimensional bounded field is required to interpret these results unambiguously.

F. Future work

In future work we will consider methods of separating the internal gradient and surface relaxation contributions to the

observed $T_{2,\mathrm{eff}}$ relaxation time distributions at high magnetic field strengths. We will also consider low-field measurements of rock cores with high concentrations of paramagnetic impurities and explore how the internal gradients influence these results. It will also be necessary to extend models of internal magnetic field profiles to three dimensions in order to further understand diffusion in the preasymptotic localization regime.

The observation of spins in a very broad distribution of pore sizes and at an intermediate magnetic field strength (in the limit that some spins are governed by MAV and others by ST) could potentially allow the pore size distribution to be divided artificially into small and large pores through the careful selection of the experimental parameters. In an ideal porous material with a bimodal pore size distribution, this would provide sufficient relaxation contrast to observe pore-to-pore exchange. However, controlling the experimental parameters for a real sample so as to define a single critical length separating arbitrary small and large pores will likely be impossible; as with the sandstone rock studied here, the existence of multiple relaxation modes in large pores will make interpretation of the results ambiguous.

VI. CONCLUSIONS

In this paper, we have explored the influence of internal gradients on $T_{2,\mathrm{eff}}$ NMR relaxation measurements by observing diffusive exchange phenomena in a water saturated sandstone across a range of magnetic field strengths. The internal gradients present in the sample were observed to scale with $B_0^{3/2}$, and T_1 relaxation times were shown to have only a weak dependence on field strength (explained by surface relaxation theory), as expected. The $T_{2,\mathrm{eff}}$ relaxation times, determined from CPMG measurements, were found to be strongly dependent on magnetic field strength. The echo time dependence of $T_{2,\mathrm{eff}}$ was explored, and this became more pronounced as the magnetic field strength increased due to diffusive attenuation in the internal gradients. Significantly, these results indicated that the internal gradients are nonuniform across an individual pore. Finally, we examined T_2-T_2 exchange plots for the same sample at different magnetic field strengths. As B_0 increased, the number of discrete $T_{2,\mathrm{eff}}$ components also increased, leading to the appearance of multiple exchange pathways. These pathways were associated with exchange between volumes of residual magnetization detected from spins diffusing in local regions of weak magnetic field gradient. Hence, intrapore (rather than interpore) exchange was observed.

For T_2-T_2 measurements of porous media in general, it is difficult to distinguish exchange pathways observed between pores and between regions of local magnetic field gradient extrema within individual pores unless a suitably low B_0 magnetic field strength can be used so as to guarantee that the observed $T_{2,\mathrm{eff}}$ relaxation time distribution reflects the pore size distribution. Exchange pathways observed in high magnetic field measurements, or in samples with intrinsic paramagnetic chemical species (and hence large internal gradients), cannot be related unambiguously with pore-to-pore exchange. Nevertheless, it may be possible to use these high-field measurements to characterize other structural parameters, such as pore size, geometry, or surface chemistry.

In general, for materials with large pores where the characteristic pore size $R>10$ μm, T_1 becomes a better indicator of the pore size distribution than $T_{2,\mathrm{eff}}$ at intermediate to high magnetic field strengths ($B_0>1$ T). Even at lower magnetic field strengths it is advisable to keep the echo time in a CPMG measurement as short as possible (say, $t_E<2$ ms), to ensure that diffusion is governed by the ST regime. Prior to interpreting T_2-T_2 relaxation data, the "data collapse" of CPMG decays acquired with a range of t_E as presented in [5] and demonstrated here in Fig. 7 should be attempted, to identify the applicable diffusion regime. The ST regime, being the ideal case for rock studies, can be identified by a successful data collapse. Generally, the data collapse fails outside of this regime. However, the results presented here suggest a successful data collapse may also be observed in the preasymptotic localization regime, but only after a significant fraction of the magnetization has been lost to diffusion. This situation can be identified by a simple comparison of initial echo amplitudes, as demonstrated in Fig. 9.

From this work, it is possible to conclude that for most rock samples, the $T_{2,\mathrm{eff}}$ distributions will only reflect the pore size distribution in low-field measurements (where the internal gradients are small), and where the echo time limit $t_E \ll \langle T_{2,\mathrm{eff}} \rangle$ can be achieved. This limit was defined in Eq. (38). These conclusions will relate to all types of saturated or partially saturated porous media studied by T_2 NMR relaxometry. Extra care must be taken when interpreting two-dimensional plots of T_2-T_2 exchange and it is important to understand the role of internal gradients in these measurements.

ACKNOWLEDGMENTS

The authors would like to thank Dr. John Crawshaw for the SEM and EDX measurements, and Mr. John Staniland for preparing the samples. For helpful discussions, we thank Dr. Martin Hürlimann, Dr. Mick Mantle, Dr. Andy Sederman, Dr. Dan Holland, and Dr. James Collins. For financial support, J.M. thanks Schlumberger Cambridge Research and T.C.C. thanks Syngenta. Additional funding was provided by the EPSRC under Grant No. EP/F047991/1.

[1] E. M. Haacke, R. W. Brown, M. R. Thompson, and R. Venkatesan, *Magnetic Resonance Imaging~Physical Principles and Sequence Design* (Wiley, New York, 1999).
[2] R. J. S. Brown, Phys. Rev. **121**, 1379 (1961).
[3] L. E. Drain, Proc. Phys. Soc. London **80**, 1380 (1962).
[4] B. Audoly, P. N. Sen, S. Ryu, and Y. Q. Song, J. Magn. Reson. **164**, 154 (2003).
[5] M. D. Hürlimann, J. Magn. Reson. **131**, 232 (1998).
[6] B. Q. Sun and K. J. Dunn, Phys. Rev. E **65**, 051309 (2002).
[7] B. J. Balcom, R. P. MacGregor, S. D. Beyea, D. P. Green, R. L. Armstrong, and T. W. Bremner, J. Magn. Reson., Ser. A **123**, 131 (1996).
[8] S. Emid and J. H. N. Creyghton, Physica B & C **128**, 81 (1985).
[9] Y. Q. Song, S. Ryu, and P. N. Sen, Nature (London) **406**, 178 (2000).
[10] N. V. Lisitza and Y. Q. Song, J. Chem. Phys. **114**, 9120 (2001).
[11] P. N. Sen, C. Straley, W. E. Kenyon, and M. S. Whittingham, Geophysics **55**, 61 (1990).
[12] Y. Q. Song, L. Venkataramanan, M. D. Hürlimann, M. Flaum, P. Frulla, and C. Straley, J. Magn. Reson. **154**, 261 (2002).
[13] M. D. Hürlimann and L. Venkataramanan, J. Magn. Reson. **157**, 31 (2002).
[14] P. T. Callaghan, S. Godefroy, and B. N. Ryland, J. Magn. Reson. **162**, 320 (2003).
[15] B. Q. Sun and K. J. Dunn, Magn. Reson. Imaging **23**, 259 (2005).
[16] K. R. Brownstein and C. E. Tarr, Phys. Rev. A **19**, 2446 (1979).
[17] S. Davies and K. J. Packer, J. Appl. Phys. **67**, 3163 (1990).
[18] K. Munn and D. M. Smith, J. Colloid Interface Sci. **119**, 117 (1987).
[19] R. L. Kleinberg and S. A. Farooqui, J. Colloid Interface Sci. **158**, 195 (1993).
[20] K. E. Washburn, C. D. Eccles, and P. T. Callaghan, J. Magn. Reson. **194**, 33 (2008).
[21] R. J. S. Brown, R. Chandler, J. A. Jackson, R. L. Kleinberg, M. N. Miller, Z. Paltiel, and M. G. Prammer, Concepts Magn. Reson. **13** (6), 344 (2001).
[22] H. Carr and E. Purcell, Phys. Rev. **94**, 630 (1954).
[23] S. Meiboom and D. Gill, Rev. Sci. Instrum. **29**, 688 (1958).
[24] E. L. Hahn, Phys. Rev. **80**, 580 (1950).
[25] M. D. Hürlimann, K. G. Helmer, T. M. de Swiet, P. N. Sen, and C. H. Sotak, J. Magn. Reson., Ser. A **113**, 260 (1995).
[26] M. D. Hürlimann and D. D. Griffin, J. Magn. Reson. **143**, 120 (2000).
[27] P. J. McDonald, J. P. Korb, J. Mitchell, and L. Monteilhet, Phys. Rev. E **72**, 011409 (2005).
[28] K. E. Washburn and P. T. Callaghan, Phys. Rev. Lett. **97**, 175502 (2006).
[29] L. Monteilhet, J. P. Korb, J. Mitchell, and P. J. McDonald, Phys. Rev. E **74**, 061404 (2006).
[30] J. Lee, C. Labadie, C. Springer, and G. Harbison, J. Am. Chem. Soc. **115**, 7761 (1993).
[31] L. Venkataramanan, Y. Q. Song, and M. D. Hürlimann, IEEE Trans. Signal Process. **50**, 1017 (2002).
[32] J. Mitchell, J. D. Griffith, J. H. P. Collins, A. J. Sederman, L. F. Gladden, and M. L. Johns, J. Chem. Phys. **127**, 234701 (2007).
[33] K. E. Washburn, C. H. Arns, and P. T. Callaghan, Phys. Rev. E **77**, 051203 (2008).
[34] M. Fleury and J. Soualem, J. Colloid Interface Sci. **336**, 250 (2009).
[35] J. A. Hornemann, S. L. Codd, K. Romanenko, and J. D. Seymour, Diffus. Fundam. **10**, 1.1 (2009).
[36] T. M. de Swiet and P. N. Sen, J. Chem. Phys. **100**, 5597 (1994).
[37] H. C. Torrey, Phys. Rev. **104**, 563 (1956).
[38] J. P. Korb, M. W. Hodges, T. Gobron, and R. G. Bryant, Phys. Rev. E **60**, 3097 (1999).
[39] W. E. Kenyon, Nucl. Geophys. **6**, 153 (1992).
[40] J. Mitchell, P. Blumler, and P. J. McDonald, Prog. Nucl. Magn. Reson. Spectrosc. **48**, 161 (2006).
[41] P. T. Callaghan, *Principles of Nuclear Magnetic Resonance Microscopy* (Clarendon, Oxford, 1991).
[42] D. C. Douglass and D. W. McCall, J. Phys. Chem. **62**, 1102 (1958).
[43] R. C. Wayne and R. M. Cotts, Phys. Rev. **151**, 264 (1966).
[44] S. D. Stoller, W. Happer, and F. J. Dyson, Phys. Rev. A **44**, 7459 (1991).
[45] P. Le Doussal and P. N. Sen, Phys. Rev. B **46**, 3465 (1992).
[46] B. Robertson, Phys. Rev. **151**, 273 (1966).
[47] P. N. Sen, A. Andre, and S. Axelrod, J. Chem. Phys. **111**, 6548 (1999).
[48] C. H. Neuman, J. Chem. Phys. **60**, 4508 (1974).
[49] L. J. Zielinski and P. N. Sen, J. Magn. Reson. **147**, 95 (2000).
[50] J. A. Glasel and K. H. Lee, J. Am. Chem. Soc. **96**, 970 (1974).
[51] R. J. S. Brown and P. Fantazzini, Phys. Rev. B **47**, 14823 (1993).
[52] Q. Chen, A. E. Marble, B. G. Colpitts, and B. J. Balcom, J. Magn. Reson. **175**, 300 (2005).
[53] M. D. Hürlimann (private communication).
[54] P. N. Sen and S. Axelrod, J. Appl. Phys. **86**, 4548 (1999).
[55] D. S. Grebenkov, J. Magn. Reson. **180**, 118 (2006).
[56] J. J. Friel and C. E. Lyman, Microsc. Microanal. **12**, 2 (2006).
[57] G. Wahba, SIAM (Soc. Ind. Appl. Math.) J. Numer. Anal. **14**, 651 (1977).
[58] J. D. Wilson, J. Mater. Sci. **27**, 3911 (1992).
[59] R. Vold, J. Waugh, M. Klein, and D. Phelps, J. Chem. Phys. **48**, 3831 (1968).
[60] J. P. Butler, J. A. Reeds, and S. V. Dawson, SIAM (Soc. Ind. Appl. Math.) J. Numer. Anal. **18**, 381 (1981).
[61] S. Godefroy, J. P. Korb, M. Fleury, and R. G. Bryant, Phys. Rev. E **64**, 021605 (2001).
[62] J. Mitchell, M. D. Hürlimann, and E. J. Fordham, J. Magn. Reson. **200**, 198 (2009).
[63] V. Anand and G. J. Hirasaki, J. Magn. Reson. **190**, 68 (2008).